國立臺灣大學理學院物理學研究所

博士論文

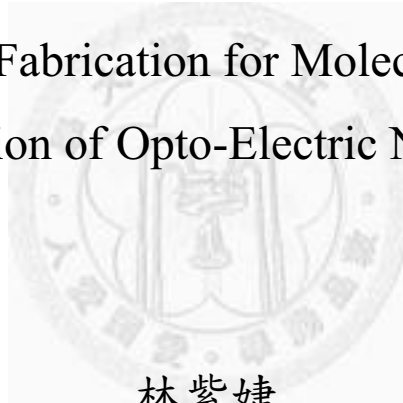Graduate Institute of Physics

College of Science

National Taiwan University

Doctoral Dissertation

製作奈米結構使分子配向於奈米光電元件之應用

Nanostructure Fabrication for Molecular Alignment

in Application of Opto-Electric Nanodevices

林紫婕

Tzu-Chieh Lin

指導教授：趙治宇 博士

Advisor: Chih-Yu Chao, Ph.D.

中華民國 99 年 7 月

July, 2010

致謝

  從大學部就開始在台大物理系，復古風格的紅磚牆舊館到火箭般的新館我都經歷，宿舍以及校園裡的每一個景致，現在看起來都益發可愛，於此我要感念國家以及學校對我的栽培。感謝從研究所便開始指導我的趙老師，他開啟了我們學生在奈米領域的新視野，教導我們研究需具有新創意，給予學生很高的自由度發揮，獲益良多。還有要謝謝我身旁的好友，大學同學及高中姊妹淘，包容我這些年減少了聯絡，但我心裡是時刻想念著各位的。再者，我要謝謝實驗室的學弟妹，菖哥、RITA、威廷、前助理怡晴、君瑋、祖銳、俊彰、謝榕、及少卜都豐富有趣了我的實驗生活，希望你們的研究也可以順利。以及感謝曾經教導過我以及關心我的系上老師，在你們忙碌之餘還經常被我叨擾，你們的研究精神及道德涵養都將使我一輩子受用。還要感謝因禱告而得到的天使Ｂ，伴我完成博士學位，於生活上亦幫助我許多，感念甚深。我要將博士學位的榮耀獻給我的爸媽及我的家人，在我情緒低落時，你們總是無限包容我，很高興我有個幸福且堅若磐石的家庭，這是什麼都換不來的。終於不負期待畢業了，真的很高興也衷心感謝，學生生涯將告一段落，今後會更以此負責對待我的研究工作以及認真的生活，無論位居社會哪一職位，我都將真誠謙虛以及懷抱熱枕貢獻我的專業。

摘要

舉凡生醫或光電等領域，分子配向一直以來均有其重要之應用性。其中製作奈米溝槽是用以導引分子使其有序排列方法之一。在本篇論文裡，我們探討了數種製作奈米結構的軟微影術，並將其應用在奈米光電元件。根據 Berreman 理論，液晶分子為使表面自由能達最小值，而沿表面溝槽方向排列。控制液晶分子之排向在液晶顯示器中扮演了舉足輕重的角色，它決定了液晶層能否成功的控制光線出入，進而成為一有效之光閥。

首先，我們使用了導電原子力顯微術 (conductive atomic force microscopy nanolithography)，外加電場於 p 型矽基板上，氧化成長無機之二氧化矽奈米溝槽，以製備反射式之液晶晶胞。原子力顯微術提供了精細之畫素與高解析度，以及能更準確的控制液晶分子的次序性。相對於一般傳統摩擦配向膜的方式，不僅免去了高溫製程，無機的配向層亦不會因摩擦產生碎屑及靜電，且可承受製程時的紫外線傷害與操作環境之高溫。適用於小尺寸面板、投影機及可攜電子式產品的應用。

本論文於第四章介紹利用創新之軟微影技術(soft lithography) - 破裂觸發自組裝溝槽 (crack induced self-assembled grooves) - 來使液晶分子配向。此方法利用高分子層內的行進波於上下基板之間來回震盪，形成正弦波的溝槽。由實驗歸納得出，溝槽的週期與高分子層的膜厚相關，約成四倍的關係，亦與理論符合。我們於本論文中做出最小約 70 nm 線寬的溝槽。

利用此方法我們可用膜厚調控溝槽週期，進而控制液晶之定錨能以及對比度，效果接近以傳統絨布摩擦 PI (polyimide)配向膜。此軟微影術提供一快速簡易且不需外加任何模子(mold)的方法，我們於本論文中介紹了技術細節以及理論運算。

最後，我們介紹了另一種特殊的軟微影方法－熱致拉引法(thermal drawing)－以製作自組裝溝槽，我們使用了具 grating 圖案的矽基板當作上模，加熱下基板之高分子，根據 ICE Model 的靜電理論，利用上模與高分子之間的靜電力拉引熔融之高分子，使之形成與上模同樣 pattern 的高分子溝槽。此方法為 AFM-assisted electrostatic nanolithography (AFMEN) 之更進階，其可免去 AFM 掃描，以提升面積與效率，且不需外加電場熔融高分子。用此方法製作溝槽來使液晶分子配向，可避免摩擦配向造成之缺陷，不僅可製成反射式液晶晶胞，也可應用在穿透式的液晶晶胞。

本篇論文介紹利用數種新穎的軟微影技術，以製作奈米級溝槽使液晶分子配向，這些方法不僅能應用在液晶顯示器，還可用於生物晶片、微流通道、積體電路、太陽能電池等生醫光電產品，於現在及未來均具有相當前瞻之應用性。

Abstract

Molecule alignment has many significant applications in biotechnology, molecular electronics, optoelectronic devices and liquid crystal (LC) displays manufacturing. Fabrication of nanogrooves is one of the approaches for ordering molecules. In this dissertation, we investigate several nanolithography generating nanostructures and apply them in opto-electric devices for liquid crystal alignment.

At first, in Chapter 3, conductive atomic force microscopy (CAFM) nanolithography was used to modify a silicon surface. This approach generating the silicon oxide grating by CAFM gives a good control of liquid crystal (LC) alignment in the micron or submicron region. It establishes a pixel with a smaller size to achieve high-resolution images. Compared with the conventional cloth rubbing and AFM scratching techniques, CAFM nanolithography prevents scratching damage, dust contamination and residual static electricity problems. Furthermore, this inorganic alignment method can also avoid the damage caused by UV light exposure and high-temperature environment. It could be applied to small panels, projectors, liquid crystal on silicon (LCOS), and portable electronics.

In Chapter 4, we employed a fast and high-throughput method, fabricating micro- and nano-grooves for the alignment of liquid crystal molecules. Splitting the polymer film sandwiched by two substrates triggers the propagating wave front to induce self-assembled grooves on the polymer surfaces. This crack-induced grooving (CIG) method not only avoids the high-temperature

process, dust and ion contaminations caused by traditional rubbing, but also provides a large anchoring energy comparable to that using polyimide rubbing. This CIG method could generate tunable-period grooves without any masks. It also offers an appealing alternative to existing technologies for LC molecules alignment.

In Chapter 5, we represented a fascinating soft lithography - thermal drawing lithography (TDL) - to fabricate self-assembled periodic grooves. The prepatterned silicon mold with protruding grating, exists a spacer gap, is placed on a bottom substrate spin-casted with polymer film. According to the image charge-induced electrohydrodynamic-instability (ICE) model, the attractive electrostatic force between upper and bottom substrates would cause heat-induced melting polymer film to rise and form a positive replica grating pattern similar to the upper mold. In our work, we confirm thermal drawing lithography could be achieved without an external electric field and prove the ICE model by experimental results. We have utilized these self-assembled grooves to align liquid crystal molecules for both reflective and transmissive liquid crystal cells.

In this dissertation, we introduce several novel soft lithography fabricating nanogrooves for liquid crystal alignment. Not only for liquid crystal displays, these approaches fabricating submicro or nano-structures provide a simple means and have great potential for many other fields, like biochips, microchannels, molecular circuits, solar cells, etc.

目　錄

Chapter 1　Introduction   1

List of Figures

List of Tables

List of Publications

Journal Papers

1. Alignment Control of Liquid Crystal Molecules Using Crack Induced Self-Assembled Grooves, Tzu-Chieh Lin, L. C. Huang, T. R. Chou, and C. Y. Chao, *Soft Matter* (Impact Factor = 4.869) **5**, 3672 (2009).

2. Fabrication of Alignment Layer Free Flexible Liquid Crystal Cells Using Thermal Nanoimprint Lithography, Tzu-Chieh Lin, S. C. Yu, P. S. Chen, K. Y. Chi, H. C. Pan, and C. Y. Chao*, Current Applied Physics* **9**, 610 (2009).

3. Fabricating Alignment-Layer Free Flexible Liquid Crystal Devices by the Replica Molding Method, P. S. Chen, H. H. Chang, J. W. Chen, Tzu-Chieh Lin , and C. Y. Chao, *Chinese Journal of Physics* **47**, 55 **(**2009).

4. Alignment Control of Liquid Crystals Using Conductive Atomic Force Microscopy Nanolithography, Tzu-Chieh Lin and C. Y. Chao*, Japanese Journal of Applied Physics* **47**, 4583 (2008).

5. To Eliminate Optical Bounce of Homeotropic Alignment Liquid Crystal Cells by Rubbing Treatment, Tzu-Chieh Lin, S. F. Liu, and C. Y. Chao. (submitted)

6. Formation of Self-assembled Periodic Grooves via Thermal Drawing Lithography for Alignment Layers in Liquid Crystal Devices, Tzu-Chieh Lin, L. C. Huang, C. C. Huang, and C. Y. Chao. (submitted)

Conference Papers

1. Liquid Crystal Alignment on Sub-Microgrooves by Using Oxidation Nanolithography, Tzu-Chieh Lin and C. Y. Chao, *Mol. Cryst. Liq. Cryst.* **510**, 134 (2009).

2. Flexible Liquid Crystal Cells without Alignment Film, Tzu-Chieh Lin, S. C. Yu, P. S. Chen, K. Y. Chi, H. C. Pan, and C. Y. Chao, *Mol. Cryst. Liq. Cryst*. **510**, 141 (2009).

3. Using Replica Molding Method to Fabricate Alignment-Layer Free Flexible Liquid Crystal Devices, P. S. Chen, H. H. Chang, J. W. Chen, Tzu-Chieh Lin, and C. Y. Chao, *Mol. Cryst. Liq. Cryst.* **507**, 194 (2009).

4. Crack Induced Self-assembled Grooves for Liquid Crystal Molecules Alignment, Tzu-Chieh Lin, L. C. Huang, T. R. Chou, and C. Y. Chao. (submitted)

5. Suppressing Optical Bounce for Homeotropic Liquid Crystal Cells by Rubbing Treatment, Tzu-Chieh Lin, S. F. Liu, and C. Y. Chao. (submitted)

Presentation at Professional Conferences

2008 International Liquid Crystal Conference (Korea, Poster presentation)

2009 The Physical Science of Republic of China (Oral presentation)

2010 The Physical Science of Republic of China (Oral presentation)
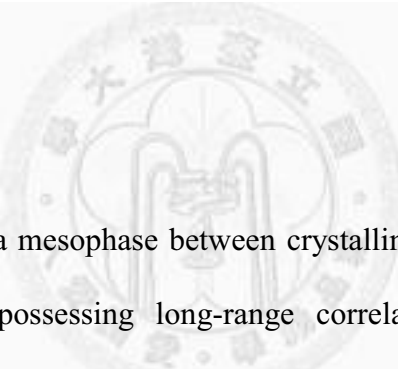
2010 International Liquid Crystal Conference (Poland, Oral presentation)

Chapter 1

Introduction

1.1 Liquid Crystals

Liquid crystal (LC) is a mesophase between crystalline solid and isotropic liquid. Liquid crystal molecules possessing long-range correlations with respect to the orientation of their molecular axes show crystal-like properties, but are still able to flow like fluid.[1,2] In 1888, liquid crystal was first discovered by the Austrian chemist Friedrich Reinitzer. He observed a turbid cloudy liquid existed between the solid crystal and a clear transparent liquid while he was heating cholesteryl benzoate and trying to measure its melting point. Until now, there are many kinds of liquid crystal molecules have been found. According to the condition of formation, they can be broadly categorized as lyotropic and thermotropic.[3]

Lyotropic liquid crystal molecules consist of a hydrophobic tail and a hydrophilic head and form liquid crystal phases when dissolved in a polar solvent (Figure 1.1). The molecules assemble to make the tails group together, exposing the hydrophilic heads to

the solvent. Phase transitions are caused by changing the solvent concentration. Thermotropic liquid crystals typically are formed from pure compounds or mixtures of rod or disc shaped molecules and their ordering is a function of temperature.
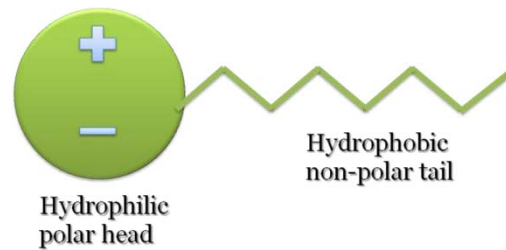
Figure 1.1 Lyotropic liquid crystal

Classified by their shapes, liquid crystal molecules could be sorted into rod-like, disk-like, banana-shaped, conical, and shuttlecock-shaped. In general, there are three liquid crystal phases, known as the smectic, nematic and cholesteric phases. Figure 1.2(a) and (b) show the phases of smectic A and C forming layered structure that can slide over one another like soap. In the smectic A phase, the molecules are oriented

(a) Smectic A   (b) Smectic C   (c) Nematic
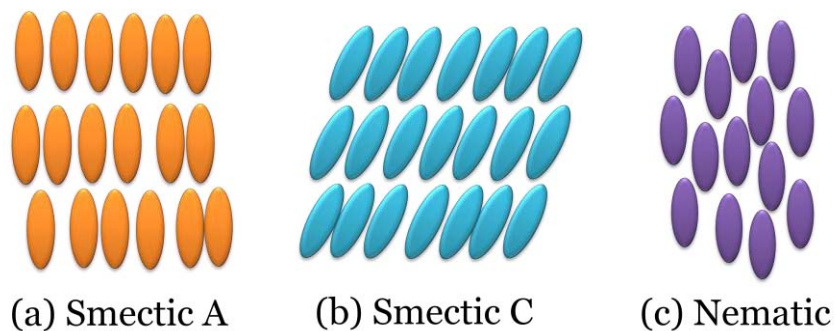
Figure 1.2 Phases of liquid crystals: (a) smectic A phase (b) smectic C phase (c) nematic phase.
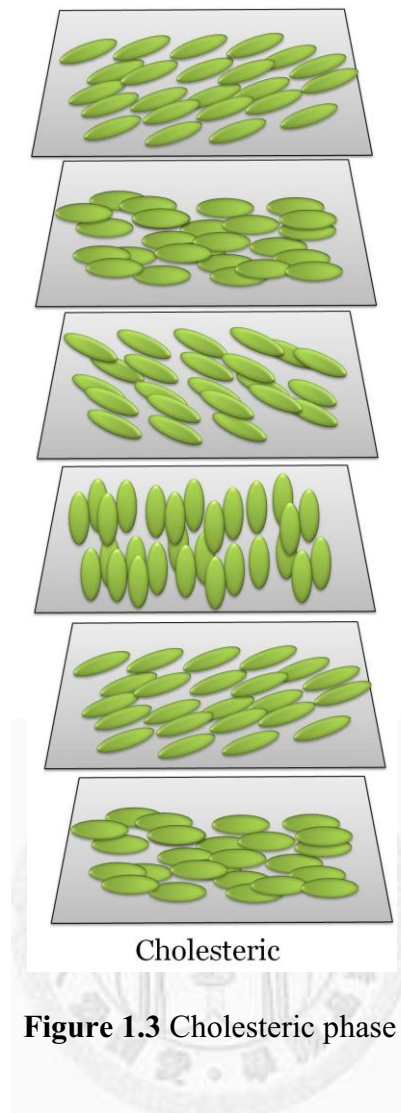
Figure 1.3 Cholesteric phase

along the layer normal, while in the smectic C phase LCs are tilted away from the layer normal. Figure 1.2(c) illustrates the nematic phase which only has the long-term ordering direction of molecular axes. Cholesteric phase is also a nematic type of LC except that it is added with chiral molecules (Figure 1.3). The cholesteric structure would spontaneously twist about a helical axis normal to the director. The distance of helix which the directors of cholesteric LCs rotate 360° is called its pitch.

For rodlike liquid crystals, the anisotropic configuration causes the birefringence

and optical anisotropy. The conjugated double bonds yield large pi electrons distributed along the long axis of the molecule. Thus polarizability differs between parallel and perpendicular to the long axes. Hence the optical properties depend on direction and polarization of the incident light, and the LC material shows birefringence. The optical anisotropy is defined as

$$\Delta n = n_e - n_o \tag{1-1}$$

where n_e is extraordinary refractive index for light with electric field polarization parallel to the director and n_o is ordinary refractive index for light with electric field polarization perpendicular to the director. If the polarized light incidents at an angle θ with the LC molecular axes, the effective refractive index should be

$$\frac{1}{n_{eff}^2(\theta)} = \frac{sin^2\theta}{n_e^2} + \frac{cos^2\theta}{n_o^2} \tag{1-2}$$

Due to the uniaxial symmetry, the dielectric constants are different for along the preferred axis ($\varepsilon_\parallel$) and perpendicular to the axis ($\varepsilon_\perp$). The dielectric anisotropy is defined as

$$\Delta\varepsilon = \varepsilon_\parallel - \varepsilon_\perp \tag{1-3}$$

If $\Delta\varepsilon > 0$, which is called positive dielectric anisotropy, LC would align parallel to the applied electric field owing to the lowest electrostatic energy. On the contrast, if $\Delta\varepsilon < 0$,

4

negative dielectric anisotropy, LC would be perpendicular to the applied electric field.

LCs possess curvature elasticity like most liquids and solids. While the system is deformed and disturbed from its equilibrium state, the elastic constants of LC determine the restoring torques. There are three basic deformations for LCs as shown in Figure 1.4. The elastic constants relative to the restoring force of LC: k_1, k_2, and k_3 are the splay, twist, and bend elastic constant, respectively. Proposed by Oseen-Frank theory, the elastic energy density of a deformed LC can be written

$$F = \frac{1}{2} \, k_1 (\boldsymbol{\nabla} \times \boldsymbol{n})^2 \; + \; \frac{1}{2} \, k_2 (\boldsymbol{n} \cdot \boldsymbol{\nabla} \times \boldsymbol{n})^2 \; + \; \frac{1}{2} \, k_3 (\, \boldsymbol{n} \times \boldsymbol{\nabla} \times \boldsymbol{n})^2 \qquad (1\text{-}4)$$

For most LCs, the elastic constant is around the order of piconewtons (10^{-12} N).
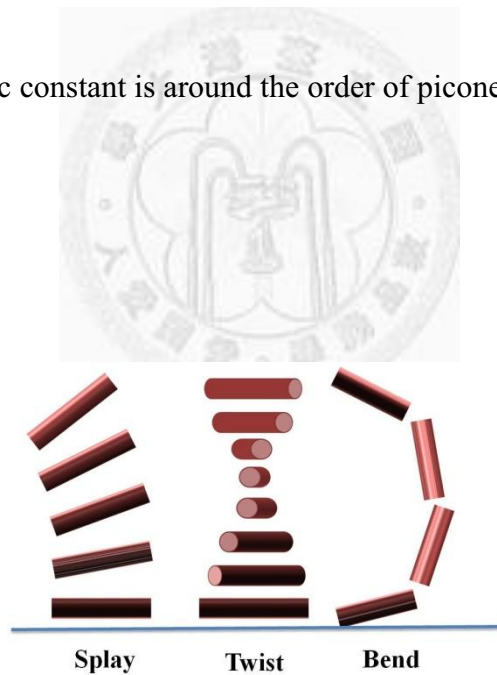
Figure 1.4 Schematic of splay, twist, and bend in LC

1.2 Twist Nematic (TN) Liquid Crystal Displays[2-4]

Twist Nematic cells are widely used for both transmissive and reflective liquid crystal displays (LCDs). These displays have well features, like high contrast ratio, low operating voltage, weak color dispersion, and fast response time. In the dissertation, both tranmissive and reflective types are used and discussed.

1.2.1 Transmissive 90° twist nematic liquid crystal displays

In a 90° TN-LC cell, the angle of the LC directors between the front substrate and the exit substrate is 90°. The incident light will follow the twist of local director as it propagates in the LC and the direction of polarization of the light is rotated by 90°. The 90° TN-LC cell is sandwiched between a pair of parallel polarizer and analyzer. The transmission axis of the polarizer at the input end is aligned parallel to the director of LC (Figure 1.5(a)). This is known as normally black (NB) mode. The LC cell is considered as a stack of wave plates and the phase retardation of the LC cell before twisted is

$$\Gamma = \frac{2\pi}{\lambda} \cdot \Delta n \cdot d \qquad (1\text{-}5)$$

where d is the thickness of the LC cell, λ is the wavelength of the incident light.

The transmission for unpolarized monochromatic light is given by

$$T = \frac{1}{2} \cdot \Phi^2 \cdot \frac{sin^2 X}{X^2} = \frac{1}{2} \cdot \frac{sin^2[\frac{\pi}{2}\sqrt{1+u^2}]}{1+u^2} \tag{1-6}$$

where $\Phi = \pi/2$ as the nematic phase twist angle between the top and the bottom substrates, $x^2 = \Phi^2 + \frac{\Gamma^2}{4}$, the Mauguin parameter u is
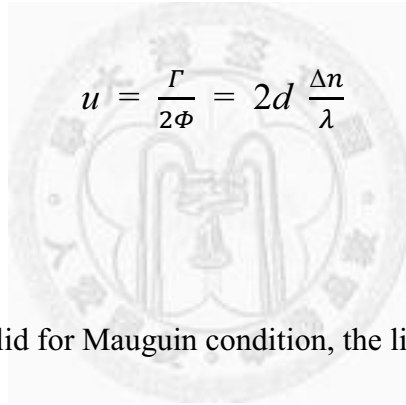
$$u = \frac{\Gamma}{2\Phi} = 2d\frac{\Delta n}{\lambda} \tag{1-7}$$

The waveguiding is only valid for Mauguin condition, the limit of slow twist.

$$\Phi \ll \Gamma = \frac{2\pi}{\lambda}\Delta nd \tag{1-8}$$

For a 90° TN-LC cell, the condition reduces to

$$\frac{\lambda}{2} \ll \Delta nd \tag{1-9}$$

Under this inequality (*u* is large), the transmission T is close to zero (i.e., normally black state). The molecular orientation of LC can be controlled to align with an applied electric field. The polarization of the incident light would not change and the state would be bright.

In normally white (NW) mode, The 90° TN-LC cell is sandwiched between a pair of crossed polarizer and analyzer. The director of LC at the input end is parallel to the transmission axis of the polarizer and the director of LC at the exit end is parallel to the transmission axis of the analyzer (Figure 1.5(b)). If an external electric field is applied, the polarization of the incident light would not change and the state would be dark.

(a) NB

(b) NW
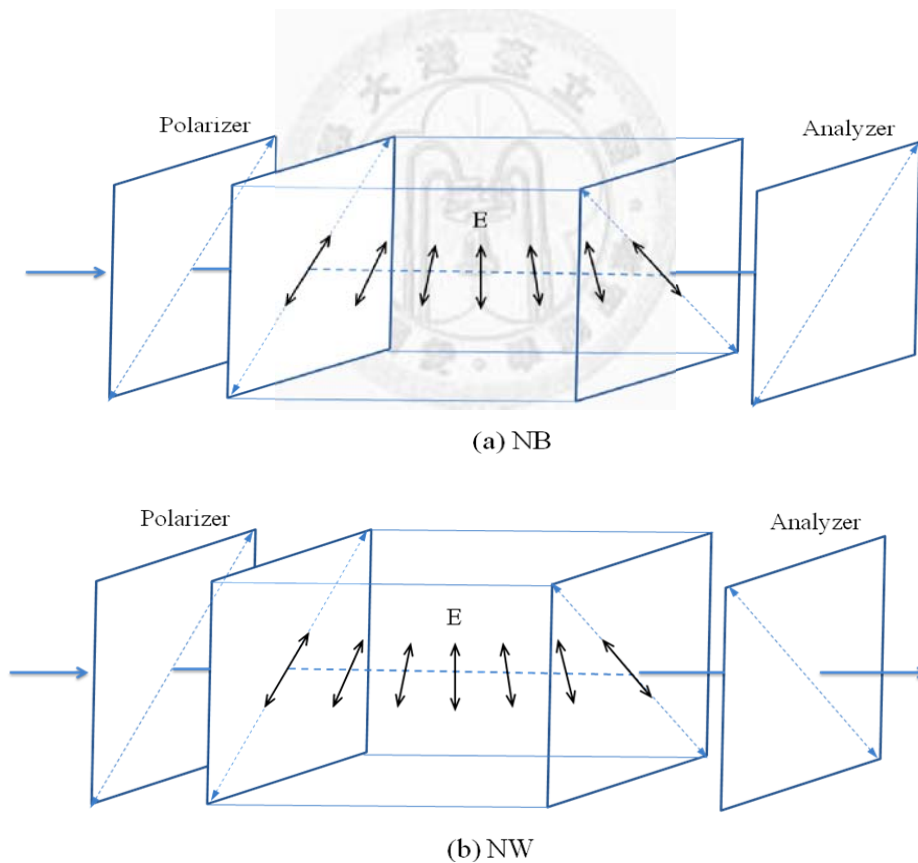
Figure 1.5 Principle of operation of 90 ° TN displays (a) NB mode (b) NW mode.

1.2.2 Reflective mixed-mode twist nematic (MTN) liquid crystal displays

The performance of a MTN cell for a reflective display is equivalent to that of a TN cell for a transmissive display. Differently, a MTN cell only requires one front polarizer to reduce the parallax. The reflectance for a MTN cell is given by

$$R = (\Gamma \frac{sin\, x}{x})^2 (sin\, 2\beta\, cos\, x - \frac{\Phi}{x} cos\, 2\beta\, sin\, x)^2 \qquad (1\text{-}10)$$

β is the angle between the polarizer axis and the front LC director. Other parameters are defined as in section 1.2.1. The reflectance depends on the angle β, twist angle Φ of LC, the light wavelength λ, LC birefringence Δn, and the LC cell gap d (λ and d are included in Γ). Control these parameters, the minimum of reflectance for a MTN-LC cell could be achieved - this is the normally black state. If an electric field is applied, LCs would align normally to the substrates and the light would not change its polarizing direction. Thus, the MTN-LC cell would become the bright state due to there is only one polarizer.

1.3 Mechanisms of Liquid Crystal Alignment

Molecular alignment has important application in many different fields, like biochips, microchannels, molecular circuits, polarizers, organic semiconductors, etc.[5-10] Especially for liquid crystal displays, alignment of LC molecules is very influential for it determines if LC system could be a successful light valve. However, the underlying

physics for LC alignment is a longstanding debate and still under investigated.[11] There are two main mechanisms proposed to explain the LC alignment. The first mechanism is to generate anisotropic molecular interaction forces between LCs and alignment layer. The second mechanism is indicated that elastic deformation of the LC configuration is due to periodic surface topologies. We will discuss these mechanisms in the following sections.

1.3.1 Anisotropic molecular interaction forces between LCs and alignment layer

Anisotropic molecular interaction forces between LCs and alignment layer is considered to dominate the LC alignment. Thus, generating elongated and stretching polymer chains is the most main purpose to achieve this mechanism. There are several methods proposed to create directional and anisotropic molecular structure or polymer chain, like Langmuir-Blodgett film, oblique evaporation, photoalignment, ion beam bombard, rubbing treatment.[12-16] Surface rubbing is the conventional way to tailor the polymer chain. But it still has some disadvantages, like debris generation, electrostatic residual, high baking temperature, etc. Thus, many researches try to improve its drawbacks or control the LC alignment through other methods. In this dissertation, we focus on fabrication of surface relief grating for ordering LCs.

1.3.2 Elastic deformation of the LC configuration by periodic surface topologies[17,18]

Based on Berreman's model, the periodic surface relief grating for governing LC alignment is assumed to be the sine wave form. Figure 1.6 demonstrates the arrangement and defined parameters of the following calculation. L is the director of LC

and the direction of grooves is parallel to y axis.

$$Z \sim A \ sin \ qx \qquad (1\text{-}11)$$

where the wave number $q = \dfrac{2\pi}{\lambda}$, A is the amplitude of the sine wave.

For minimizing the surface energy, the azimuthal φ obeys the following equation

$$\frac{\partial^2 \varphi}{\partial x^2} \ + \ \frac{\partial^2 \varphi}{\partial z^2} \ = \ 0 \qquad (1\text{-}12)$$

where φ is the angle between the x-z projection of L and x axis.
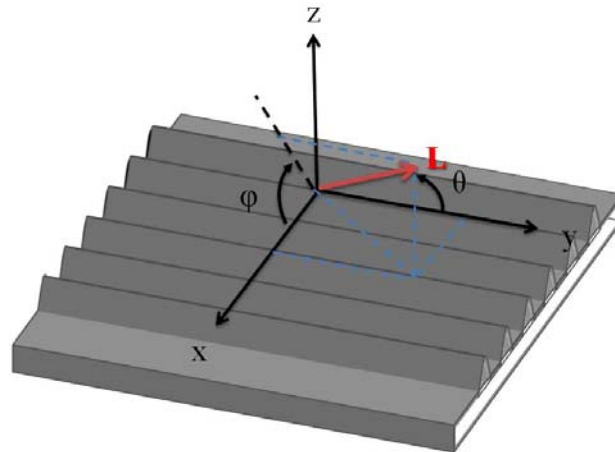
Figure 1.6 The schematic of Berreman's grooving model.

After solving the differential equation (1-12), a solution φ is found to match a gratinglike boundary and have the cosine wave form.

$$\varphi(x,z) = Aq \; cos \; (qx) \; e^{\;-qz} \tag{1-13}$$

The cosine function could be derived from sine function by differentiation. That means the xz-projection is tangent to the grating curve. In addition, if θ is small, for planar alignment, LCs would tend to orient parallel to the grating direction for the surface energy is minimum. The energy density due to the elastic stain is

$$u_\perp \; = \; \frac{k_3}{2} \; [(\frac{\partial\varphi}{\partial x})^2 \; + \; (\frac{\partial\varphi}{\partial z})^2] \; = \; \frac{k_3}{2} \; (Aq)^2 q^2 \; e^{\;-2qz} \tag{1-14}$$

and the total energy per unit area, which is most confined within a distance $(2q)^{-1}$ of the surface, is

$$\rho_\perp = \int_0^\infty u_z dz = \frac{1}{4} \; k_3 A^2 q^3 \tag{1-15}$$

u and ρ represent the extra elastic energy,

$$u(z, \theta) = u_\perp(z) \; sin^2\theta \tag{1-16}$$

$$\rho(\theta) = \rho_\perp \; sin^2\theta \tag{1-17}$$

If θ is 0° or 180°, the elastic energy comes to the lowest and LCs would like to align to the grating direction. $\rho_\perp$ is so called the anchoring energy per unit area (f), is

$$f = \frac{1}{4} k_3 A^2 q^3 \qquad (1\text{-}18)$$

The anchoring energy density f could be controlled by changing the amplitude A and the period λ. If the anchoring energy is large, it is the nature that LCs would spontaneously have the parallel orientation for obtaining the lower energy.
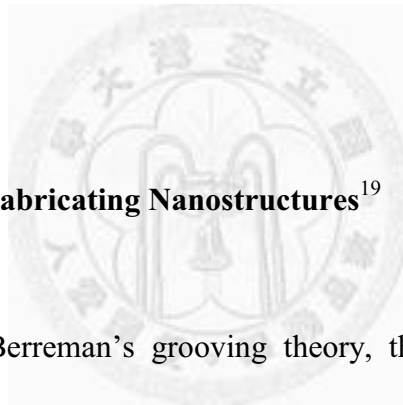
1.4 Soft Lithography for Fabricating Nanostructures[19]

In order to achieve Berreman's grooving theory, there are many technologies proposed to fabricate micro- or submicro-grooves for aligning LCs. In the following, we will discuss several soft lithography try to generate polymer grooves for application in many interdisciplinary fields.

1.4.1 Replica Molding (REM)[20]

Replica molding is an efficient method for the faithful duplication of the surface of a mold. After pouring UV- or thermally curable prepolymers onto the mold, the prepolymers are cured to become solid. Therefore, they possess almost the same dimensions and topologies as the nanostructures in the mold (as shown in Figure 1.7(a)).

These physical interactions - van der Waals force, kinetic factors, and interfacial energy - are short-range and allows more accurate replication of small (<100 nm) features. This dimension is difficult for photolithography due to the optical diffraction.[21] The low-cost replica molding generates reliable duplication of three-dimensional complex structures in a single step. Replica molding could be applied against a rigid mold, like silicon substrate, usually pouring with a thermoplastic polymer for the mass-production of a wide range of structured surfaces such as compact disks (CDs), diffraction gratings, and microdevices.[21-23] This procedure could be extended by molding against elastomeric PDMS molds rather than rigid molds; the use of elastomers makes it easier to release small and fragile structures.

1.4.2 Microtransfer Molding (μTM)[24]

In μTM (Figure 1.7(b)), a thin layer of liquid prepolymer is casted on the patterned surface of a PDMS mold by spin coating or pouring. If needed, the excess liquid could be removed by scraping with a flat block or by blowing off with a stream of nitrogen. This mold, with the prepolymer filled in the empty between the nanostructures, is then placed in contact with the surface of a substrate, and then prepolymer is cured to a solid by exposuring the sample to UV light or heating it. When the PDMS mold is peeled away carefully, a patterned microstructure is left on the surface of the substrate. If the patterned surface is used to be a resist of etching, the residual polymer between the designed nanostructures must be removed by using O_2 plasma-etching process leaving the rare surface of the substrate. Especially, the polymers for μTM could be pristine, doped with fluorescent dyes, or organic polymers. Besides, μTM can also form three-dimensional microstructures layer by layer.
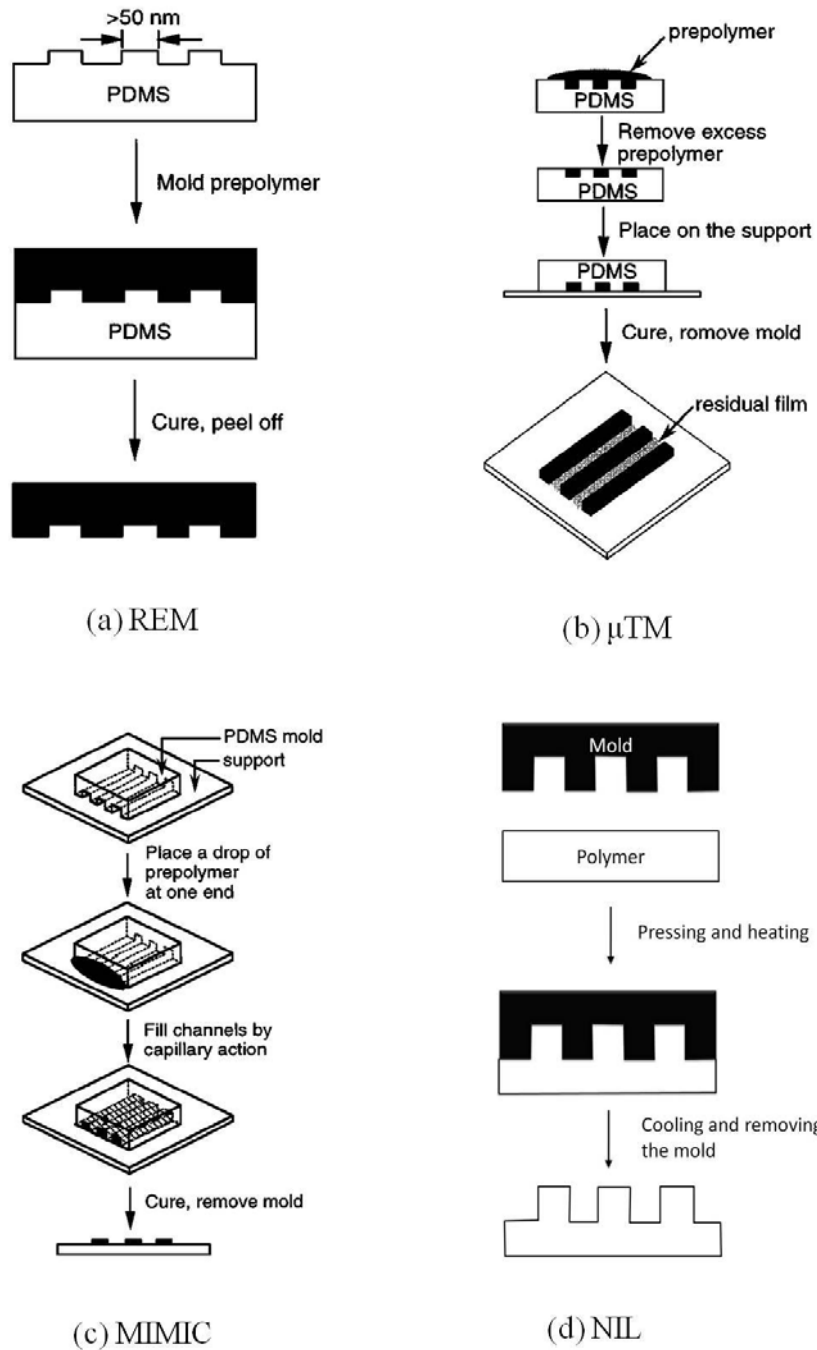
Figure 1.7 ((a)-(c) is excerpted from ref. 18) The flowcharts of (a) Replica molding (b) Microtransfer Molding (c) Micromolding in Capillaries (d) Nanoimprint lithography.

1.4.3 Micromolding in Capillaries (MIMIC)[25]

In MIMIC (Figure 1.7(c)), a patterned PDMS mold is placed on the surface of a substrate to form a network of empty channels between them. After placing a low-viscosity prepolymer at the open ends of the channels, the liquid would spontaneously fill the channels by capillary force. Then the prepolymer is cured into a solid, the PDMS mold is peeled to leave only patterned polymer microstructures. The materials of solution could be a great diversity, like UV-curable or thermally curable prepolymers that have no solvents, solutions of functional polymers, sol-gel materials, inorganic salts, polymer beads, colloidal particles, and biologically functional macromolecules.[26-27] When the solvents are evaporated, the materials in the solutions solidify to be confined within the channels and form patterned microstructures on the surface of the substrate. MIMIC forms microstructures in a single step, whereas photolithography requires several complex steps of patterning. If a Si/SiO$_2$ substrate was used for MIMIC, a free-standing microstructure of polyurethane could be created by dissolving the substrate in an aqueous HF/NH$_4$F solution to lift off the layer of SiO$_2$. Choosing suitable solution of polymer, MIMIC could make multilayer-microstructures.

1.4.4 Nanoimprint lithography (NIL)[28]

Fig. 1.7(d) shows the flowchart for the thermal-NIL process. The mold for NIL in this study is the silicon wafer with micro- or nano-grooves. The silicon mold is placed on the polymer film. Then they are pressed together under a uniform pressure and heated slightly above the T$_g$ of polymer. By means of thermal-NIL technique, the microgroove pattern can be directly transferred on the plastic substrate. The simplicity of the nanoimprint technique has enabled nanoscale patterning with ultrahigh

resolutions. Nanoimprinting can not only create resist patterns, as in lithography, but can also imprint various polymers in functional devices, which can lead to a wide range of applications in electronics, photonics, and biotechnology.

References
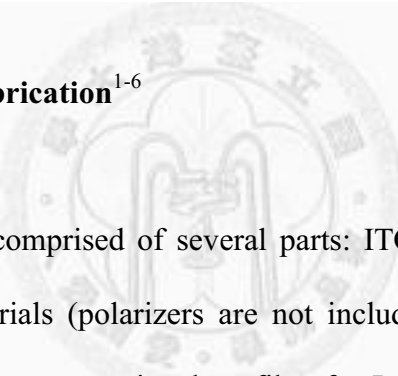
1 G. H. Heilmeier and L. A. Zanoni, *Appl. Phys. Lett.* **13**, 91 (1968).

2 P. Yeh and C.Gu, *Optics of Liquid Crystal Displays*, ed. J. W. Goodman, John Wiley & Sons, Inc. (1999).

3 G. Stojmenovik, Ion Transport and Boundary Image Retention in Nematic Liquid Crystal Displays, Universiteit Gent (2004).

4 S. T. Wu, D. K. Yang, *Reflective Liquid Crystal Displays*, ed. A. C. Lowe, Wiley-SID (2001).

5 G. M. Whitesides, E. Ostuni, S. Takayama, X. Jiang, and D. E. Ingber, *Annu. Rev. Biomed. Eng.* **3**, 335 (2001).

6 P. L. Burn, A. B. Holmes, A. Kraft, D. D. C. Bradley, A. R. Brown, R. H. Friend, and R. W. Gymer., *Nature* **356**, 47 (1992).

7 Y. Xia, M. Mrksich, E. Kim, and G. M. Whitesides. *J. Am. Chem. Soc.* **117**, 9576 (1995).

8 R. Service, *Science* **278**, 383 (1997).

9 H. A. Stone, A. D. Stroock, and A. Ajdari, *Annu. Rev. Fluid Mech.* **36**, 381 (2004).

10 K. Mizoguchi and E. Hasegawa, *Polym. Adv. Technol.* **7**, 471 (1996).

11 S. Ishihara, *J. of Display Technol.* **1**, 1 (2005).

12 M. Murata, H. Awaji, M. Isurugi, M. Uekita, and Y. Tawada, *Jpn. J. Appl. Phys.* **31**, no. 2B, L189 (1992).

13 W. Urbach, M. Boix, and E. Guyon, *Appl. Phys. Lett.* **25**, 479 (1974).

14 M. Schadt, K. Schmitt,V.Kozinkov, and V. Chigrinov, *Jpn. J. Appl. Phys.* **31**, 2155 (1992).

15 P. Chaudhara, J. A. Lacey, S.-C. A. Lien, and J. Speidell, *Jpn. J. Appl. Phys.* **37**, L55 (1998).

16 C. Mauguin, *Bull. Soc. Fr. Min.* **34**, 71 (1911).

17 F. C. Frank, *Discuss. Faraday Soc.* **25**, 19 (1958).

18 D. W. Berreman, *Phys. Rev. Lett.* **28**, 1683 (1972).

19 Y. Xia and G. M. Whitesides, *Annu. Rev. Mater. Sci.* **28**, 153 (1998).

20 Y. Xia, E. Kim, X. -M. Zhao, J. A. Rogers, M. Prentiss, and G. M. Whitesides. *Science* **273**, 347 (1996).

21 G. Wuff, *Angew. Chem. Int. Ed. Engl.* **34**, 1812 (1995).

22 H. C. Haverkorn von Rijsewijk, P. E. J. Legierse, and G. E. Thomas, *Philips Tech. Rev* **40**, 287 (1982).

23 D. A. Kiewit. *Rev. Sci. Instrum.* **44**, 1741 (1973).

24 X. -M. Zhao, Y. Xia, and G. M. Whitesides, *Adv. Mater.* **8**, 837 (1996).

25 E. Kim, Y. Xia, and G. M. Whitesides, *Nature* **376**, 581 (1995).

26 E. Kim, Y. Xia, and G. M. Whitesides, *J. Am. Chem. Soc.* **118**, 5722 (1997).

27 E. Delamarche, A. Bernard, H. Schmid, B. Michel, and H. A. Biebuyck, *Science* **276**, 779 (1997).

28 S. Y. Chou, P. R. Krauss, and P. J. Renstrom, *J. Vac. Sci. Technol., B* **14**, 4129 (1996).

Chapter 2

Experimental Methods

2.1 Liquid Crystal Cell Fabrication[1-6]

Traditional LCDs are comprised of several parts: ITO glasses, alignment layers, spacers, liquid crystal materials (polarizers are not included here for fabricating LC cells). Figure 2.1 shows the cross-sectional profile of a LC cell which is not to scale. Actually glass substrates are the thickest part (~1 mm) of a LC cell, while the LC layer is the thinnest part (about several micrometers). The following is the steps and brief discussions for fabricating a conventional transmissive LC cell. The flowchart is represented in Figure 2.2.

Fabrication steps of a transmissive LC cell:

I.   Prepare ITO glasses: In manufacturing liquid crystal displays, indium tin oxide (ITO) glasses are most usually used substrates. After cleaning ITO glasses, baking

the ITO glasses to dry the excess water thin film on the surface of glasses is important for the next step of casting polyimide (PI) due to PI would easily deteriorate under a high relative humidity (RH).

II. Spin coat PI: PI is the common alignment layer for LCDs. Bake an ITO glass casted with a PI layer at temperature around 200~250 ℃ to solidify the alignment layer. This baking temperature is pretty high for plastic substrates. This is one of the main drawbacks that we try to improve in this dissertation.

III. Rub the alignment layer: Velvet is utilized to rub PI surface for generating nanogrooves. Surface rubbing treatment is the conventional way to create nanogrooves for giving a control of LC alignment. However, it has some inevitable disadvantages, like dust generation, electrostatic residual, insufficient aligning homogeneous, and scratching defects.

IV. Spray spacers: Glassy spherical spacers sprayed on the bottom substrate separate the upper and bottom glass substrates and sustain the cell gap of the cell. The diameter of the spacers determines the cell gap, it is often about several micrometers.

V. Assemble and seal the cell: Put the upper substrate with the same process from step I to III onto the bottom substrate with spacers. (Rubbing directions of the two substrates are perpendicular for a TN-LC cell.) Seal the upper and bottom substrates together with UV glue which would be solidify under illumination of UV light.

VI. Fill LC materials: Due to the cell gap is narrow, once LCs are placed on one of the open end, they would fill the cavity of the cell.

VII. Seal the open ends of the cell with UV glue.

Figure 2.1 The cross-sectional profile of a transmissive LC cell.
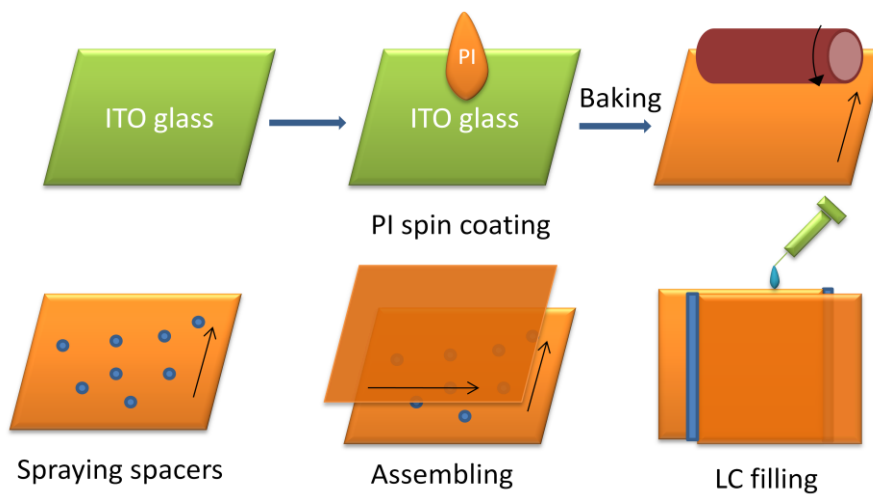
Figure 2.2 The flowchart of fabricating a LC cell.

Figure 2.3 shows the cross-sectional profile of a reflective MTN cell. Except for the rear substrate is a silicon substrate in this dissertation, other parts are similar to those in a transmissive LC cell. The details of fabricating a MTN cell will be introduced in the following chapters respectively.

Figure 2.3 The cross-sectional profile of a reflective MTN-LC cell.

2.2 Electro-optical Measurement

We introduce a method to measure the transmission of the TN-LC cell. The sample is mounted between two crossed polarizers. The easy axis of the front substrate is parallel to the polarizer and the director of LC at the exit end is parallel to the transmission axis of the analyzer (Figure 2.4). Before applying an electric field, it is the bright state - normally white. He-Ne laser at 632.8 nm is used to be the incident light source. It is important to notice and check that the light need to incident normally to the surfaces of the sample and polarizers. Then the alternating current (AC) with frequency 1 kHz is applied to the upper and bottom ITO substrates of the sample. As the applied voltage increasing, the transmission-voltage (T-V) curve performs as a function of the

applied voltages as shown in Figure 2.5. While the applied voltage is higher than threshold voltage (V_{th}), the director of LC begins to change its direction and tends to align parallel to the electric filed. Thus it becomes the dark state and the transmission decreases. The light intensity is measured by the photodetector.
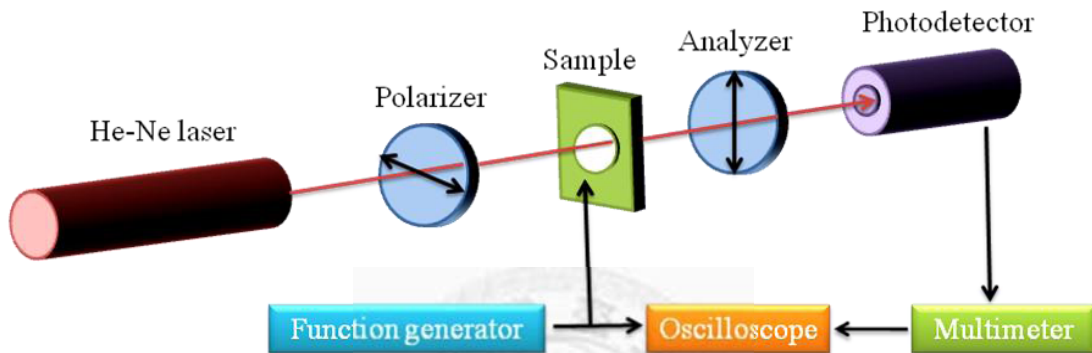
Figure 2.4 The experimental setup for the T-V curve measurement.
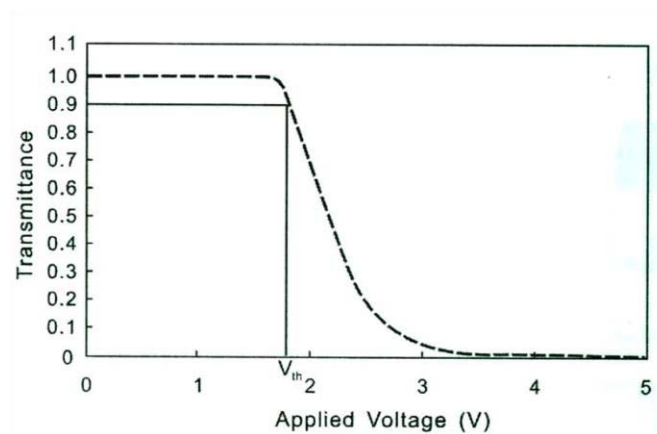
Figure 2.5 An illustration of T-V curve of a TN cell with NW mode.

In this dissertation, we employ doped and polished silicon substrates as rear substrates. Thus, the rear substrate could combine the function of an electrode and an mirror. Different from a transmissive LC cell, the incident light passes through the MTN cell twice. And the polarizing beam splitter (PBS) is needed while measuring the reflectance-voltage (R-V) curve. PBS could be replaced by a beam splitter (BS) and a polarizer. Then the output light is separated from the incident light. Rotate the polarizer to get the extreme darkness (for NB mode) and record the output light. The experimental setup is shown in Figure 2.6.
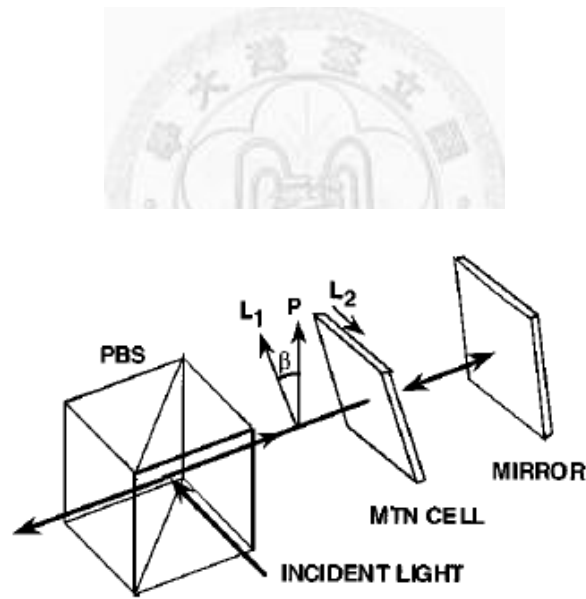
Figure 2.6 (this figure is excerpted from ref. 6) Experimental configuration of a 90° MTN cell: PBS is the polarizing beam splitter; P is the polarization axis; L_1 and L_2 are LC alignment directions at the front and rear substrates, respectively; and β is the angle between L_1 and P.

According to the Electro-optical (EO) curve, we could calculate the contrast. It is defined as the ratio of the transmission of the bright state to that of the dark state.

$$C_{NW} = T_{NW}(0) \; / \; T_{NW}(V) \qquad\qquad (2\text{-}1)$$

where T_{NW} is the transmission of the TN cell with NW mode.

References

1 P. Yeh, C. Gu, *Optics of Liquid Crystal Displays*, ed. J. W. Goodman, John Wiley & Sons, Inc., US 1999.

2 A. Lien and H. Takano, *J. Appl. Phys.* **69**, 1304 (1991).

3 H. Kim and Y. H. Lee, *Applied Optics* **44**, 1642 (2005).

4 H. C. Chang, Master Thesis, N. T. U. Taiwan (2008).

5 S. T. Wu, D. K. Yang, *Reflective Liquid Crystal Displays*, ed. A. C. Lowe, Wiley-SID, UK 2001, p. 89–108.

6 S. T. Wu and C. S. Wu, *Appl. Phys. Lett.* **68,** 1455 **(**1996).

Chapter 3

Alignment Control of Liquid Crystals Using Conductive

Atomic Force Microscopy Nanolithography
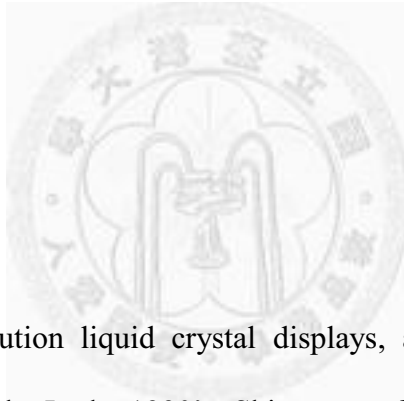
3.1 Introduction

To achieve high-resolution liquid crystal displays, alignment control of liquid crystal plays a significant role. In the 1990's, Shigeno *et al.* utilized scanning tunneling microscopy (STM) to observe the configuration of LC on the graphite surface.[1] Concerning the interaction energy between the substrate and molecules, they constructed models for liquid crystal arrangement. For LCDs, the main mechanism responsible for azimuthal LC alignment is proposed to be surface grooves based on Berreman's continuum theory.[2] For nowadays mass production, conventional rubbing by cloth is widely used for LC alignment. But cloth rubbing is insufficient to dominate the LC orientation in the micron or submicron domain. To improve this drawback, Rüetschi *et al.* scratched the polymer surface by atomic force microscopy (AFM).[3] More than successfully aligned LCs, they developed an optical waveguide of one low

effective refractive index in the middle of two high index domains resulting from two different AFM writing directions. There are many other researches using the AFM scratching technique for LC alignment in the past few years.[4–7] Wen *et al.* fabricated the LC cell with gray scale by rotating the AFM scratching direction across the adjacent stripe regions.[5] Kim *et al.* used the AFM stylus to perform an in-plane surface multistability due to the multi-fold rotational symmetry of the pattern.[6] They also proposed that LC pretilt angle is a function of line density scratched by AFM.[7] However, both of cloth rubbing and AFM scratching techniques may produce scratching damage, dust contamination and residual static electricity on the polyimide substrates. In addition, the scratching method is quite harmful to the stylus of AFM.

Here we demonstrate a method using conductive AFM (CAFM) to generate periodical SiO_2 grating on a doped silicon surface for LC alignment.[8–10] The CAFM nanolithography enables us to govern precisely the direction and the line separation of the SiO_2 grating as it is required. We find this approach generating the silicon oxide grating by CAFM can anchor the directions of LCs on the substrate and gives a control of LCs alignment in the micron or submicron region. According to the Frank elastic energy theory, the global configuration of LC direction is parallel to the surface-relief grooves to minimize orientational distortion.[11] Moreover, this inorganic LC alignment method using CAFM not only avoids the drawbacks caused by conventional cloth rubbing and AFM scratching techniques, but also establishes a pixel with a smaller size to achieve high-resolution images. Furthermore, unlike PI alignment layer, the inorganic LC alignment method by CAFM can avoid damage generated by long-time UV light exposure and high-temperature environment in LCD projector.

3.2 Experiments

3.2.1 CAFM nanolithography

In our experiments, the silicon wafers used for AFM writing are p-type (resistivity 1-20 Ω cm), and oriented in (100) direction. This wafer is conductible and polished so as to be used as a reflector. Thus a parallax problem occurring when the reflector is placed behind the rear substrate could be averted.[12] The wafers were cleaned by ethanol in an ultrasound cleaner for 5 min and subsequently rinsed by deionized water. After cleaning, for H-passivated surface, the samples were dipping in 10% HF solution by 60 s.[8-9] The wafers were cleaned again by the above steps and purged by nitrogen gas. Then the surface preparation was completed for CAFM writing. CAFM nanolithography was carried out in air using Veeco CP-R microscope with the AFM tip (Ultrasharp) coated with Cr/Au conductive film and operated in the contact mode.
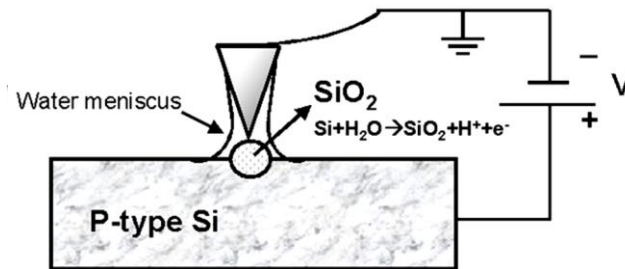
Figure 3.1 Schematic of the CAFM system.

In writing SiO_2 pattern, the protruding lines were generated when a positive bias was applied on the silicon substrate at a voltage above 5 V and the AFM tip was grounded. Figure 3.1 represents the architecture of CAFM system. This nanolithography

utilizes a thin layer of absorbed water covering on the sample and the tip.[13] The CAFM

nanolithography was performed at the speed 1 μm/s with the density of 2.5 lines/μm.

All the lithography process was done at room temperature with an ambient relative

humidity of approxmiately 60%. The topography image of SiO_2 line pattern was taken

by AFM at scanning rate of 6 μm/s with the same tip when zero voltage was applied to

the silicon substrate [see Fig. 3.2(a)]. As shown in Fig. 3.2(b), the substrate bias of 7 V

gives oxidation width of 250 nm and height of 7 nm approximately. Figure 3.2(c) taken

by scanning electron microscope (SEM) shows the SiO_2 grating generated at bias

voltage of 8 V. The variation of oxidation height vs. voltage V is demonstrated in Fig.

3.3. The height of oxidation increases with the applied bias voltage.
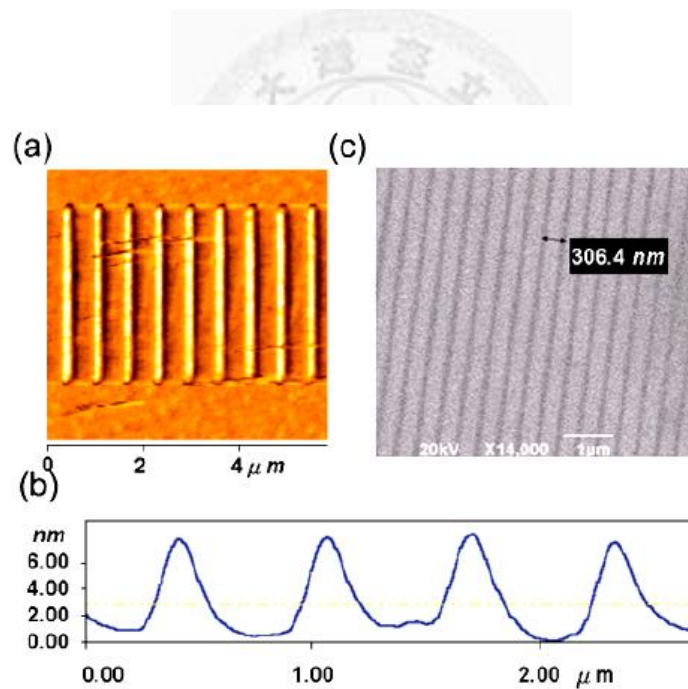
Figure 3.2 (a) The AFM image of SiO_2 grating line pattern.

(b) The height profile of a SiO_2 grating line.

(c) SEM image of SiO_2 grating.
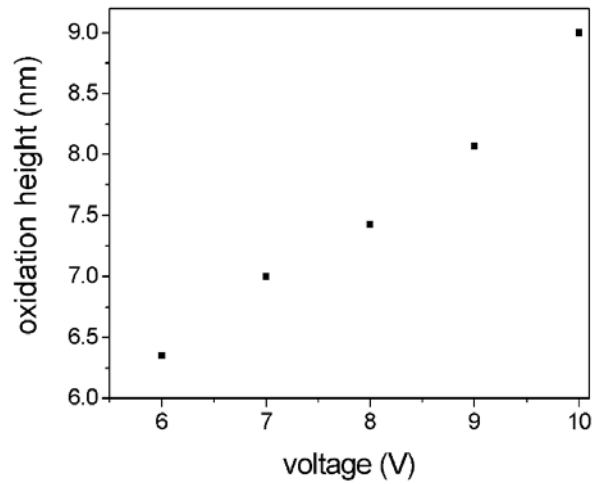
Figure 3.3 The variation of oxidation height h vs. voltage V. The height of oxidation increases with the applied bias voltage.

3.2.2 Fabrication and measurements of LC cells

The silicon substrate patterned by CAFM was placed opposite the conventionally rubbed PI layer which was grown on top of an ITO coated glass substrate. Then, we filled the empty cell with a 4-n-pentyl-4'-cyanobiphenyl (5CB) LC at room temperature. The PI rubbing direction on the counter surface was set orthogonal to the CAFM writing direction. Therefore, the director configuration of LCs sandwiched between the SiO_2 patterned substrate and rubbed PI layer became 90° twisted and the background was homogeneous. The cells are inspected by a polarizing optical microscopy in the reflection mode and the polarizer setting is demanded to obtain maximum brightness with zero voltage between the substrates (see Fig. 3.4). The patterned area of the cell belongs to normal white. The bright region has size of 10×20 μm^2 as shown in Fig. 3.4. The polarizer setting makes the polarizer and the LC director near the upper substrate not parallel but with some angle to form a mixed-mode twisted nematic (MTN) LC cell.

In direct-view display, the MTN LC cell requires only one front polarizer to prevent the parallax.

Utilizing the conductivity of the doped silicon, the p-type silicon we used here was not only to be an anode but also a driving electrode. The doped and polished silicon substrate patterned by CAFM can thus be simultaneously used for LC alignment, cell electrode, and mirror reflector. Applying the voltage between the ITO and p-type silicon substrates above 4 V, the patterned area of the cell, i.e., normally white mode, started to change its phase retardation. While the applied voltage was increased, the image became darker as shown in Fig. 3.4. Figure 3.5 demonstrates the voltage-dependent light reflectance of the reflective MTN LC cell. At voltage around 7.5 V, the phase retardation came into π resulting in the cell being the black state. Based on Berreman's groove model,[2] the contribution of morphology to anchoring energy is given by $W = 2\pi^3 A^2 K / \lambda^3$, where A is the amplitude, λ is the pitch of the surface corrugation, and K is the Frank elastic constant of the LC. With A ~7 nm, λ ~400 nm, and $K_{5CB} = 2 \times 10^{-12}$ N, we obtain the anchoring energy of SiO_2 grating is 9.5×10^{-8} N/m (~10^{-7} N/m) which is in the same order of AFM rubbing result.[7]
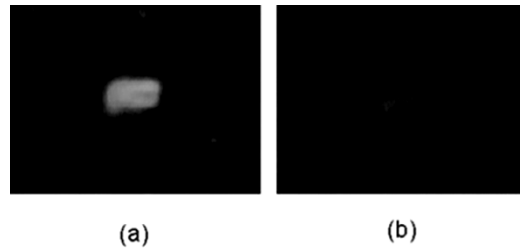
Figure 3.4 Polarizing optical micrograph of the reflective LC cell. The bright region has

size of $10 \times 20\ \mu m^2$.

(a) The bright state with zero voltage.

(b) The dark state with voltage at 7.5 V.
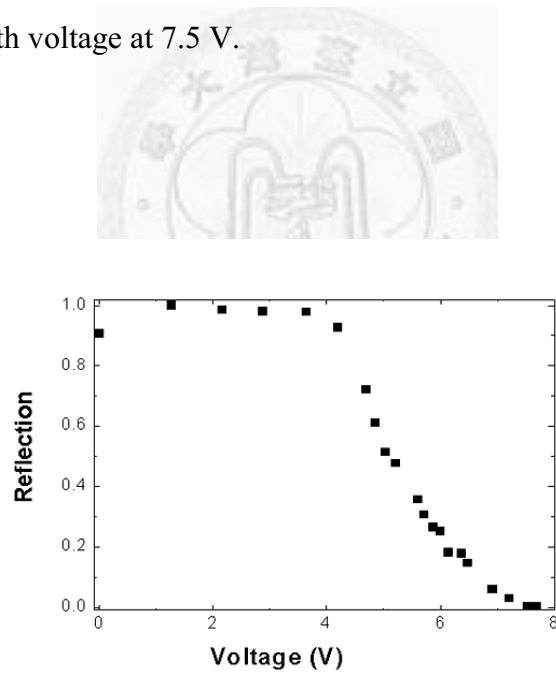
Figure 3.5 The voltage-dependent light reflectance of a MTN LC cell. The LC cell

switches to its gray scale when the applied voltage is above 4 V. Increasing the voltage

to ~7.5 V, the cell becomes dark.

3.3 Summary

In conclusion, we have shown that the silicon surface relief grating of SiO_2 by CAFM could anchor LC molecules on the substrate in order directly. The CAFM nanolithography could reduce the size and separation of the pixels in micron or submicron scale to obtain higher resolution for future LCD application. More importantly, this inorganic LC alignment method by CAFM not only prevents scratching damage, dust contamination and residual static electricity caused by conventional cloth rubbing and AFM scratching techniques, but also avoids damage generated by long-time UV light exposure and high-temperature environment in LCD projector. Finally, employing massive parallel AFM nanolithography with 55,000 styli proposed by Mirkin *et al*.[14] makes high throughput and shorter writing time possible in the future LCD application.
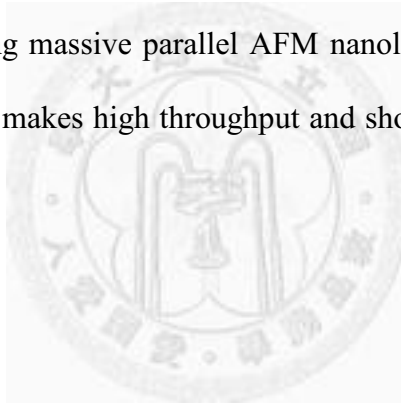
References

1 M. Shigeno, W. Mizutani, M. Suginoya, M. Ohmi, K. Kajimura, and M. Ono, *Jpn. J. Appl. Phys.* **29**, L119 (1990).

2 D. W. Berreman, *Phys. Rev. Lett.* **28,** 1683 (1972).

3 M. Rüetschi, P. Grütter, J. Fünfschilling, and H.-J. Güntherodt, *Science* **265**, 512 (1994).

4 A. J. Pidduck, S. D. Haslam, G. P. Bryan-Brown, R. Bannister, and I. D. Kitely, *Appl. Phys. Lett.* **71**, 2907 (1997).

5 B. Wen, M. P. Mahajan, and C. Rosenblatt, *Appl. Phys. Lett.* **76**, 1240 (2000).

6 J. H. Kim, M. Yoneya, and H. Yokoyama, *Nature* **420**, 159 (2002).

7 J. H. Kim, M. Yoneya, J. Yamamoto, and H. Yokoyama, *Nanotechnology* **13**, 133 (2002).

8 L. Tsau, D. Wang, and K. L. Wang, *Appl. Phys. Lett.* **64**, 2133 (1994).

9 D. Wang, L. Tsau, and K. L. Wang, *Appl. Phys. Lett.* **65**, 1415 (1994).

10 K. Matsumoto, *Oyo Buturi* **67**, 176 (1998) [in Japanese].

11 F. C. Frank, *Discuss. Faraday Soc.* **25**, 19 (1958).

12. S. T. Wu, D. K. Yang, *Reflective Liquid Crystal Displays*, ed. A. C. Lowe, Wiley-SID, UK 2001, p. 89–108.

13 H. Sugimura and N. Nakagiri, *Jpn. J. Appl. Phys.* **34**, 3406 (1995).

14 K. Salaita, Y. Wang, J. Fragala, R. A. Vega, C. Liu, and C. A. Mirkin, *Angew. Chem., Int. Ed.* **45**, 1 (2006).

Chapter 4

Crack Induced Self-assembled Grooves for Liquid Crystal Alignment
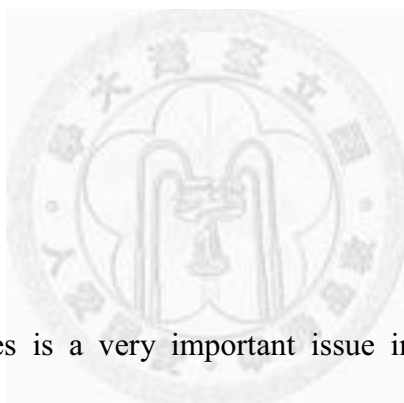
4.1 Introduction

Aligning LC molecules is a very important issue in manufacturing LCDs and devices. It is well understood that LC molecules would tend to orient along the direction of a groove due to the minimization of LC elastic energy on the groove surface.[1] Although traditionally PI rubbing is the most common technique for creating grooves on a polymer surface, and in turn renders LCs to align parallel to the groove's direction, it still has many intrinsic disadvantages like the high-temperature process (~250 ℃), dust contamination, electrostatic problems, and many ions caused by rubbing. E-Beam lithography and AFM nano-rubbing have been also utilized to tailor the polymer surface with nano-grooves for LC alignment, but the region of the pattern is very small and these techniques show a very low throughput.[2,3] Besides that, nanoimprint lithography and photolithography (PL) were employed to transfer grooves on polymer thin film for

aligning LC molecules.[4,5] However, both NIL and PL need a prefabricated mask and the period of the grooves is also limited.

In this dissertation, we propose a straightforward method, splitting a polymer film sandwiched by two substrates, for fabricating micro- or nano-grooves to align LC molecules. Figure 4.1 shows the scheme of this crack-induced grooving (CIG) method
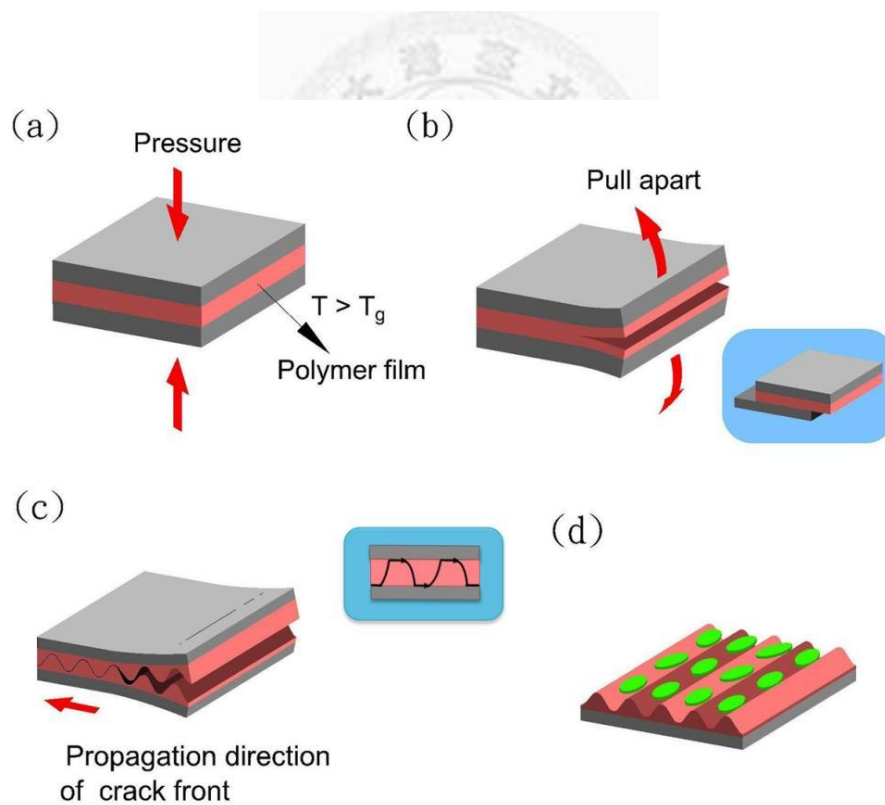
Figure 4.1 Schematic of the self-assembled grooves formation using the CIG method.

which comprises several steps. In our experiment, strong adhesion between polymer and substrates is influential in forming grooves, but do not affect the period of grooves. As shown in Fig. 4.1(a), pressing and heating the sandwiched polymer between two substrates improves the adhesion. Pulling apart the two substrates applies a driving force which would create a sufficiently large tensile stress to trigger the crack. (Fig. 4.1 (b)) When the crack edge approaches the stiff surface of the substrate, it would be reflected back into the middle of the polymer. Then the crack is confined within the polymer film and vibrates back and forth between the two substrates so as to relieve the largest tensile stress in its path (see Fig. 4.1(c)).[6] The crack front propagating from one edge to the other of the substrate brings out self-assembled grooves parallel to it. Fig. 4.1(d) demonstrates the schematic of LC molecules mainly aligning parallel to the self-formed grooves. In our experiments, we have found that the wavelength of periodic grooves is around four times the initial thickness of the thin film which is consistent with that of a previously published report.[7] The smallest period is ~150 nm and this CIG method potentially provides the possibility of reaching a smaller period by reducing the film thickness. In this work, the period is tuned for changing anchoring energy to improve the contrast ratio (CR) and the measured opto-electrical curve is comparable to that of traditionally reflective LC cells. Additionally, the anchoring energy of the self-assembled grooves is ~10^{-5} N m^{-1} which is quite close to the value using PI rubbing. This CIG method generating grooves from a featureless film is low-cost and simple. Moreover, it provides a much more rapid and larger-domain patterning method than E-beam and AFM lithography. Compared to conventional cloth rubbing and AFM scratching, this CIG method inducing self-assembled grooves also circumvents grazing damage, dust contamination and residual static electricity problems. Especially for LC devices with plastic substrates, it performs a much lower processing temperature which

is incapable by PI rubbing. The CIG method not only offers an appealing alternative to existing technologies for LC molecules alignment but also promises to be applied to the roll-to-roll process in the future.

4.2 Experiments and discussions

4.2.1 Sample preparation

For the CIG method, amorphous polymer consisting of glassy material is essential to the formation of self-assembled grooves. During the cracking, the amorphous polymer, which is noncrystalline and has no-long range molecular order, would create grooves with the same shape across a large area. On the contrary, a polycrystalline material would hamper the formation of self-assembled grooves owing to its anisotropic property. In our experiments, we choose polystyrene (PS, with a molecular weight of $M_w = 1.5$ kg mol^{-1}) which is a linear homopolymer dissolved in the toluene solvent (0.5 - 2 % solution by weight). During spin coating, the volatile toluene solvent would evaporate. Baking the substrates a little over the toluene's boiling point ($T_b = 110$ ℃) could facilitate removal of the solvent. It deserves to be mentioned that clean substrates and steady casting are required to achieve a flat film in experiments. Because dust or nonuniform polymer thickness would not only cause the wave front to change its propagating direction but also induce different pattern rather than grooves. Fig. 4.2(a) shows that a nonuniform polymer film after splitting would result in flower-like pattern, which is similar to the results made by lithography induced self-assembly (LISA).[8,9]
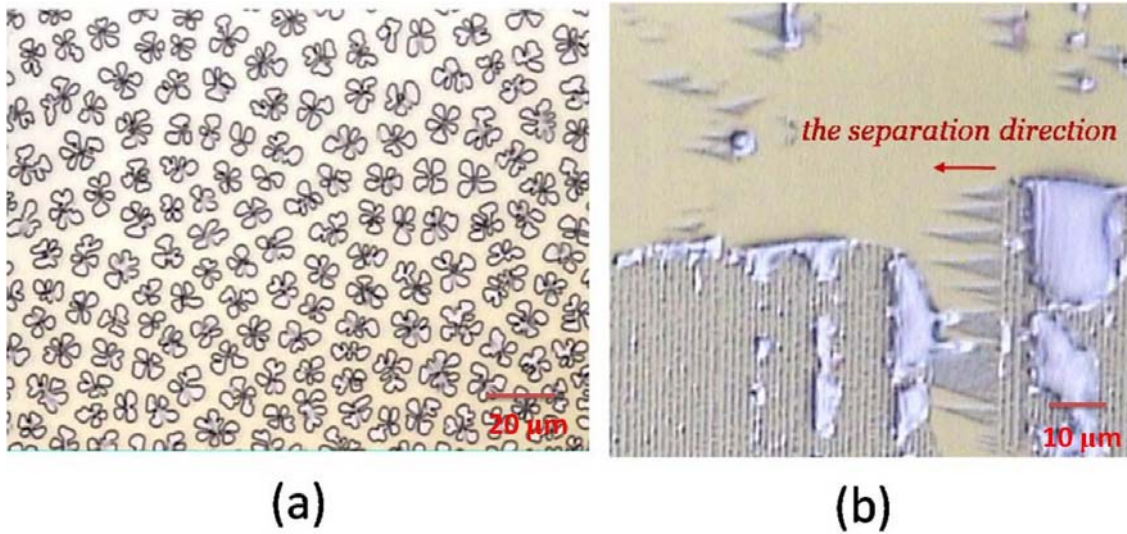
Figure 4.2 (a) The flower pattern generated by lithography induced self-assembly (LISA) (b) The separation direction is perpendicular to the direction of grooves. This result supports the model that the propagating separation wave front induces self-assembled grooves.

Although it is also a very interesting issue, we still need to focus on the CIG method for LC alignment and avoid the LISA phenomenon in this work. After casting uniform polymer film on a silicon substrate, we overlaid this substrate with the other bare substrate. Apply pressure while heating the whole sandwich structure at temperature T ~140 ℃ simultaneously. A temperature a little higher than the glass transition temperature of PS (T_g = 115 ℃) could change the glassy PS film into a rubbery film. Pressing and heating cause polymer film to attach more strongly to the substrate. If the adhesion is not enough, the separation through cracking would occur in the interface between the PS film and silicon surface, not within the PS film, then grooves would not form. Increasing the adhesive force would extend the area of pattern of the grating for

several centimeters or even larger. The applied heat and pressure were released after 10 min. The important point is that sample separation must be at the temperature below T_g of polymer. In Fig. 4.2(b), the small mark of triangular shape represents the direction of the crack which appears if the sample is not cooled down while the separation has occurred. If the separation temperature was higher than T_g, self-assembled grooves would not appear due to the rubbery polymer film, which is easily deformed. In light of the experimental results, we find that the propagating direction is perpendicular to the grooves which is consistent with the earlier results proposed by Chai and Fleck *et al.*[10,11] After being cooled down to room temperature (~25 ℃), the PS film becomes brittle and the sample was fractured into two pieces to result in the formation of polymer grooves with the complementary shape on each substrate. Fig. 4.3 shows the optical micrograph of CIG grating (period ~800 nm) across a large area. In the following, we measure the details of self-assembled grooves by AFM and SEM.
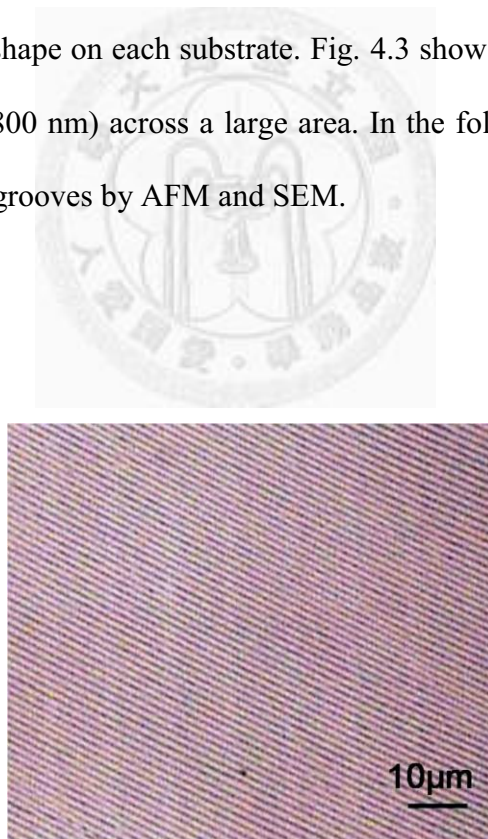
Figure 4.3 Optical micrograph of self-assembled grooves with period ~800 nm from a 200 nm thickness PS film after using the CIG method.

4.2.2 Measurements of self-assembled polymer grooves

Varying the concentration of PS toluene solution from 0.5% to 2% could get different PS film thickness after casting at the fixed frequency. The frequency of spin coating could not be too low, otherwise it would cause a nonuniform polymer film with radial distribution. As shown in Table 4.1, each concentration corresponds to a respective range of thin film thickness. A more dilute PS solution would result in a thinner film. However, the thinner film takes more attention to control the quality of film uniformity. In our work, the smallest film thickness is 35 nm from 0.5% PS toluene solution. By increasing the concentration of solution to 2%, the film thickness comes up to around 245 nm. Due to the sample arrangement is a little misfit-layered, we could easily split the attached sample apart into two substrates both with polymer grooves on the surfaces. The grooves on bottom and upper silicon substrates are nonsymmetrical, but complementary with the same period. Fig. 4.4 is the complementary grooves with period ~600 nm on the each substrate. The morphology of the PS film was inspected by AFM; the obtained period and height of grooves correspond to each different film thickness (see Fig. 4.5). With regards to Fig. 4.5, when the polymer thickness are 150, 180, and 190 nm, the pitch of grooves are about 590, 732, and 755 nm, and the height are 35, 100, and 80 nm respectively. The height is not exactly equal to the film thickness. It depends on the path of the vibrating crack front and is mostly around the half of thickness or even smaller. In this work, we observe that adhesion or annealing temperature would not affect the period of grooves, while it merely determines whether grooves would form or not. We found the period p of self-assembled grooves solely depends on the film thickness d and the period is around four times the thickness which is in consistent with Chou's work.[7,12] Hence the period could vary by adequately tuning the film thickness.

Table 4.1 The film thickness as a function of the solution concentration (with the same frequency of spin coating).

The concentration of PS toluene solution (by weight)	Film thickness
0.5%	~35 nm
1%	~85 nm
1.5%	~135 nm
2%	~245 nm
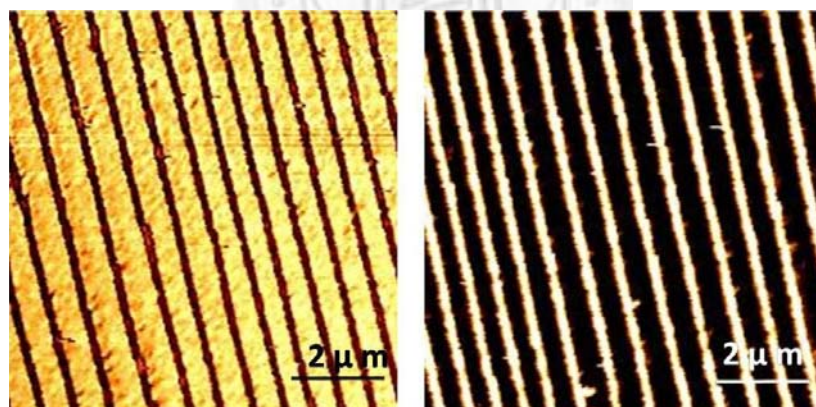
Figure 4.4 The two AFM images are surface morphology of polymer grooves from the upper and bottom substrates of the same sample after splitting. The grooves on each substrate are nonsymmetrical but complementary and with the same period (~600 nm).
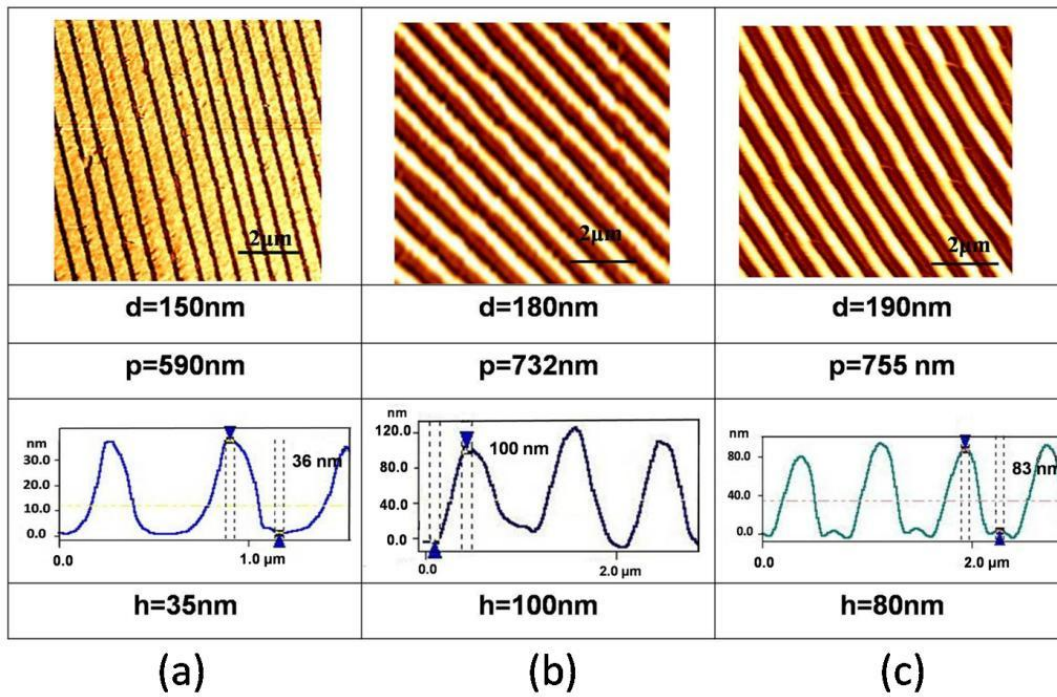
Figure 4.5 AFM measurement of the period and height of some self-assembled grooves.
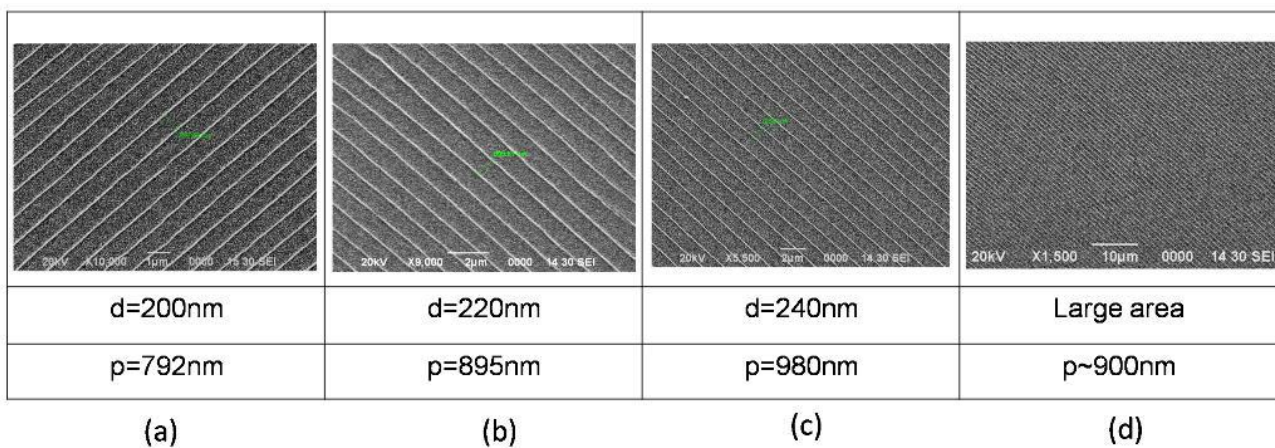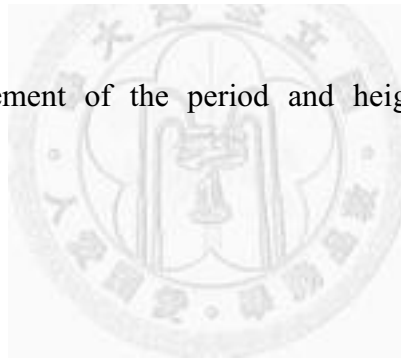
Figure 4.6 SEM micrographs of the self-assembled grooves with different periods (PS film is coated with gold film).

Fig. 4.6 represents SEM photographs of PS grooves of four different periods. Before taking SEM photographs, sputtering of a gold thin film on the PS surface is needed to prevent PS from melting at a high local energy. From Fig. 4.6(a) to (c), the period is about 792, 895, 980 nm formed in film thicknesses of 200, 220, 240 nm, respectively. Fig. 4.6(d) demonstrates a self-assembled groove across a large area (p ~900 nm). According to the AFM and SEM results, we have found the groove period p is a function of film thickness d. Fig. 4.7 demonstrates the relationship between period p and thickness d. By varying the PS concentration as mentioned above, the obtained film thickness ranges from 35 nm to 245 nm. We measured the period p of grooves is from 150 nm to 960 nm. The upper limit of the concentration in our work is 2% which results in a polymer film of about 245 nm in thickness. However, for sufficient alignment in LC devices, the period of grooves should be controlled below the LC correlation length (~1 μm).[13]
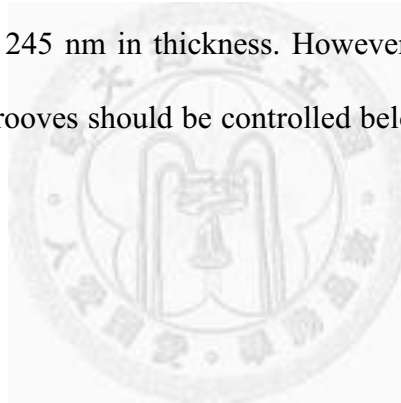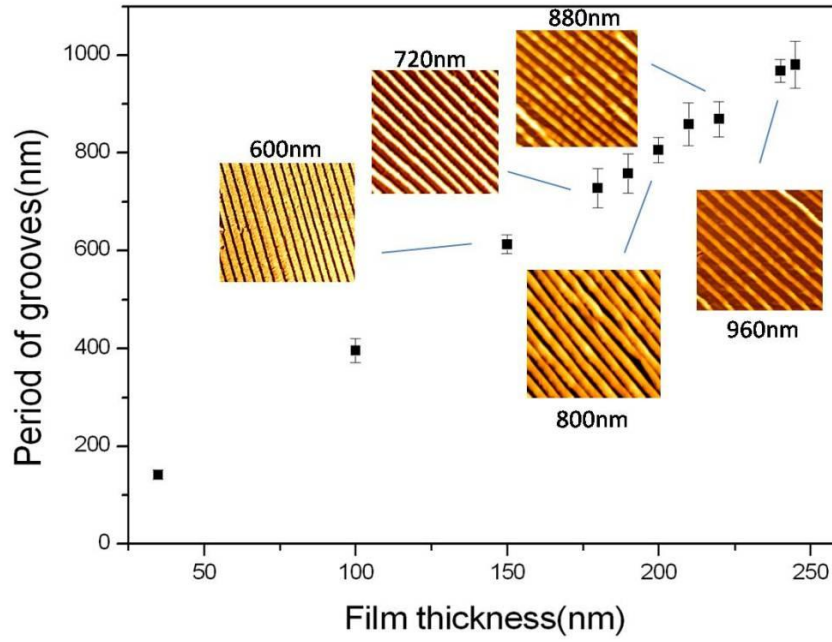
Figure 4.7 Period of grooves as a function of polymer film thickness. (The insets are AFM images and the width of each inset is 10 μm.) By controlling the film thickness from 35 nm to 245 nm, we found the period of grooves could vary from ~150 nm to ~1 μm.

4.2.3 Theory of crack induced self-assembled grooves

Based on Navier's equations (4-1) and (4-2), the polymer film is balanced by the attracting force - van der Waals force and the repulsive force - elastic force (Figure 4.8).

$$- \frac{\partial p}{\partial x} + \frac{E}{3} \frac{\partial^2}{\partial z^2} u_x(x,z) = 0 \qquad (4\text{-}1)$$

$$- \frac{\partial p}{\partial z} + \frac{E}{3} \frac{\partial^2}{\partial x^2} u_z(x,z) = 0 \qquad (4\text{-}2)$$

where u is the displacement, E is elastic constant, p is the total pressure from van der Walls force (p_v) and elastic force (p_{elas}),

$$p = p_v + p_{elas} \tag{4-3}$$

Combine Navier's equation and continuity equation (4-4),

$$\frac{\partial}{\partial x} u_x(x,z) + \frac{\partial}{\partial z} u_z(x,z) = 0 \tag{4-4}$$

We could get the displacement of x and z:

$$u_x = \frac{-3}{2E} \frac{\partial p}{\partial x} (hz - z^2) \tag{4-5}$$

$$u_z = \frac{3}{2E} \frac{\partial^2 p}{\partial x^2} (\frac{hz^2}{2} - \frac{z^3}{3}) \tag{4-6}$$

where h is film thickness of the separation point.
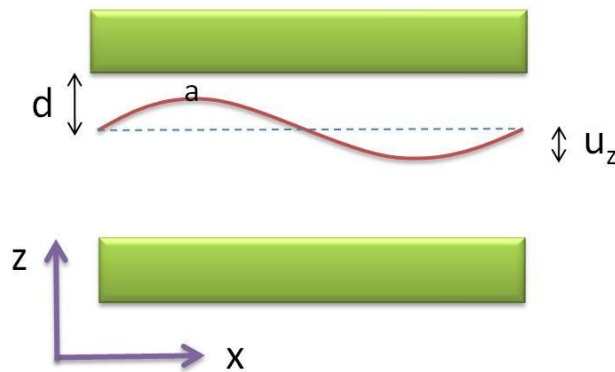
Figure 4.8 The schematic of the crack induced grooving theory.

Consider to u_z, $z = h$:

$$u_z(h) = \frac{3}{2E} \frac{\partial^2 p}{\partial x^2} \frac{h^3}{6} \qquad (4\text{-}7)$$

van der Waals force (for point a)

$$F = \frac{1}{6\pi} \frac{A}{(d-u_z)^3} = \frac{1}{6\pi d^3} \frac{A}{(1-\frac{u_z}{d})^3}$$

$$\sim \frac{A}{6\pi d^3} \left(1 - \frac{3u_z}{d}\right) \qquad (4\text{-}8)$$

where
$$p = p_v + p_{elas} = \frac{A}{6\pi d^3} \left(1 - \frac{3u_z(x,z)}{d}\right) - \frac{Eu_z}{h} \qquad (4\text{-}9)$$

Thus,

$$\frac{\partial^2 p}{\partial x^2} = \frac{-3A}{6\pi d^4} \frac{\partial^2 u_z}{\partial x^2} \qquad (4\text{-}10)$$

Inserting (4-10) into (4-7), u_z has the following form

$$u_z = \frac{3}{2E} \frac{-3A}{6\pi d^4} \frac{\partial^2 u_z}{\partial x^2} \frac{h^3}{6} \qquad (4\text{-}11)$$

$$\Rightarrow \frac{d^2 u_z}{dx^2} + \left(\frac{2}{h^2}\right) \left(\frac{2E/3h}{A/6\pi d^4}\right) u_z = 0 \qquad (4\text{-}12)$$

49

According to Shenoy's calculation for small perturbation, the critical condition for the instability taking place is

$$2E/3h \sim A/6\pi d^4 \tag{4-13}$$

$$\Rightarrow \frac{d^2 u_z}{dx^2} + \left(\frac{2}{h^2}\right) u_z = 0 \tag{4-14}$$

After solving this differential equation,

$$u_z = A sin \frac{\sqrt{2}}{h} x \tag{4-15}$$

u_z has the sine wave form and the period λ is

$$\lambda = \sqrt{2}\pi h \sim 4.4h \tag{4-16}$$

The period of the sinusoidal wave is around 4 times the film thickness which is consistent with our experimental results.

4.2.4 Fabrication and measurements of liquid crystal cells

We utilized a silicon substrate with crack-induced polymer grooves as the bottom substrate which was then covered by a conventional ITO glass coated with PI planar alignment layer as the upper substrate. The direction of crack-induced grooves was set

orthogonal to the PI rubbing direction on the opposite substrate. Then, we filled this empty cell with a 5CB LCs at room temperature and the cell gap is 1.5 μm. Therefore, the director configuration of LCs sandwiched between the crack-induced groove substrate and rubbed PI layer becomes twisted by 90°. The cells are inspected by a polarizing optical microscope in its reflection mode and the polarizer setting is demanded to obtain maximum darkness with zero voltage for the LC cell (see Fig. 4.9(a)). Thus, the patterned area (period ~800 nm, height ~100 nm) of the cell belongs to normal black. The polarizer setting makes the polarizer and the LC director near the upper substrate with some angle to form a MTN-LC cell.[14] In direct-view display, the MTN-LC cell requiring only one front polarizer could thus prevent the parallax. The doped and polished silicon substrate patterned by crack-induced self-assembled grooves could thus be simultaneously used for LC alignment, the cell electrode and the mirror reflector. Applying the voltage between the ITO and p-type silicon substrates, the patterned LC cell, i.e. normally black mode, started to change its phase retardation and became brighter as shown in Fig. 4.9(b).

(a)   (b)
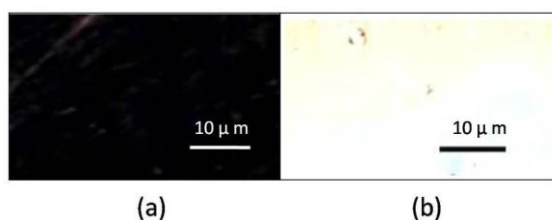
Figure 4.9 The crack-induced self-assembled PS grooves are employed to align LC molecules and used to fabricate LC cells as MTN cells. Under polarizing optical microscope, (a) is the NB state with zero applied voltage and (b) is the bright state with bias voltage ~6 V.
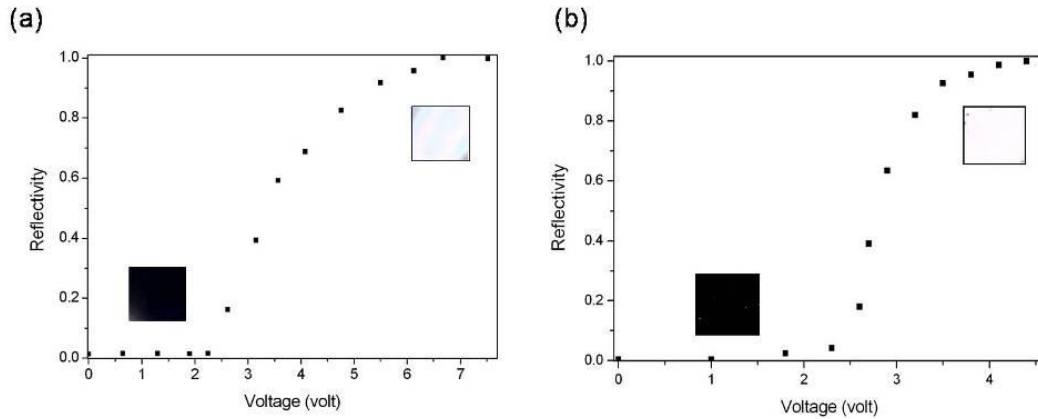
Figure 4.10 Reflectivity of MTN cells with different groove periods. (The insets are micrographs under polarizing optical microscope.) (a) The period of grooves is ~800 nm and the height is ~85 nm. (b) The period of grooves is ~600 nm and the height is ~100 nm. The calculated anchoring energy of (b) (W ~10^{-5} N m^{-1} is higher than that of (a) (W ~10^{-6} N m^{-1} and the contrast ratio of (b) (CR ~350) is better than that of (a) (CR ~75).

Fig. 4.10 demonstrates the voltage-dependent light reflectance (RV curve) of the reflective MTN LC cell. Comparing Fig. 4.10(a) and (b), the threshold voltages of these two RV curves are both around 2.3 V, because the threshold voltage is mainly determined by the LC material.[15] Increasing the applied voltage, the phase retardation came into p resulting in the cell being the bright state. According to Berreman's theory,[16] the anchoring energy resulted from grooves is W = $2\pi^3 A^2 K/ \lambda^3$, which A is the amplitude, λ is the period of groove, and K is the Frank elastic constant of the LC (K$_{5CB}$ = 2×10^{-12} N). For a MTN-LC cell in Fig. 4.9(a), with λ ~800 nm and A ~100 nm, the

anchoring energy W is ~2.4×10^{-6} N m^{-1}. For the other MTN cell in Fig. 4.10(b), with λ ~600 nm and A ~85 nm, the anchoring energy W is ~4.1×10^{-6} N m^{-1} which is ~1.7 times that in Fig. 4.10(a). The larger anchoring energy mooring LC molecules more strongly should improve the dark state and thus achieve a higher contrast ratio (CR) in LC device. In our experiments, we found that the CR of the MTN-C cell in Fig. 4.10(b) is about 350, which is five times larger than that in Fig. 4.10(a) (CR only ~75), and this result coincides with the calculated anchoring energy. Nowadays, the anchoring energy of conventional PI rubbing is 10^{-4}~10^{-5} N m^{-1} and for AFM rubbing is ~10^{-6} N m^{-1}.[17,18] As already stated, the anchoring energy of crack-induced polymer grooves is ~10^{-5}Nm^{-1}, which is an order of magnitude between PI and AFM rubbing. This anchoring energy of the PS self-assembled grooves is enough to give a good control of LC molecules.
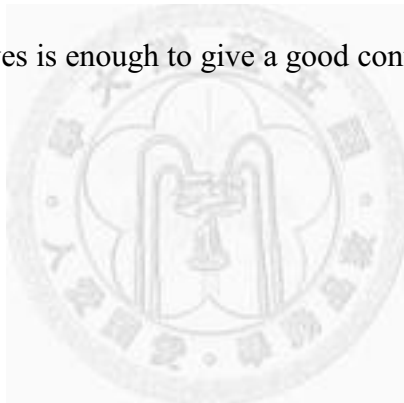
4.3 Summary

We have utilized an express and high-throughput method for LC alignment. More than successfully aligning LCs, the CIG method generates self-assembled grooves also enables alignment of other molecules, such as dyes and biomolecules, for optoelectronic devices and cell adhesion applications, etc.[19,20] In our experiment, the measured period of the grooves is found to be proportional to the film thickness. Thus, the period could be tuned as required via changing the film thickness. The anchoring energy of the crack induced grooves approaches that of conventional PI rubbing. This cutting edge method is low cost, has a low process temperature, has no dust contamination, no residual static electricity, and holds the promise of patterning self-formation grooves on glass or

plastic substrates for LCD applications. It provides an alternative comparable to the existing mainstream LCD technologies and enables application to roll-to-roll processes in the future.

References

1 F. C. Frank, *Discuss. Faraday Soc.* **25**, 19 (1958).

2 D. M. Tennant, T. L. Koch, P. P. Mulgrew, R. P. Gnall, F. Ostermeyer, and J. -M. Verdiell, *J. Vac. Sci. Technol.*, *B* **10**, 2530 (1992).

3. J. H. Kim, M. Yoneya, and H. Yokoyama, *Nature* **420**, 159 (2002).

4. S. Y. Chou, P. R. Krauss, and P. J. Renstrom, *Science* **272**, 85 (1996).

5. K. O. Hill, B. Malo, F. Bilodeau, D. C. Jackson, and J. Albert, *Appl. Phys. Lett.* **62**, 1035 (1993).

6. B. Freund, *Nat. Nanotechnol.* **2**, 537 (2007).

7. L. F. Pease III, P. Deshpande, Y. Wang, W. B. Russel and S. Y. Chou, *Nat. Nanotechnol.* **2**, 545 (2007).

8. S. Y. Chou and L. Zhuang, *J. Vac. Sci. Technol.* **17**, 3197 (1999).

9. J. Peng, Y. Han, Y. Yang, and B. Li, *Polymer* **44**, 2379 (2003).

10. H. Chai, *Int. J. Fracture* **32**, 211 (1986).

11. N. A. Fleck, J. W. Hutchinson, and Z. Suo, *Int. J. Solids Structures* **27**, 1683 (1991).

12. P. A. Deshpande, PhD Dissertation Princeton University (2005).

13. A. Rastegar, M. Skarabot, B. Blij, and Th. Rasing, J. *Appl. Phys.* **89**, 960 (2001).

14. S. T. Wu, D. K. Yang, *Reflective Liquid Crystal Displays*, ed. A. C. Lowe, Wiley-SID, UK 2001, p. 89-108.

15. X. Nie, R. Lu, H. Xianyu, T. X. Wu, and S. T. Wu, *J. Appl. Phys.* **101**, 103110 (2007).

16. D. W. Berreman, *Phys. Rev. Lett.* **28**, 1683 (1972).

17. H. Yokoyama, *Mol. Cryst. Liq. Cryst.* **165**, 265 (1988).

18. J. H. Kim, M. Yoneya, J. Yamamoto, and H. Yokoyama, *Nanotechnology* **13**, 133 (2002).

19. P. L. Burn, A. B. Holmes, A. Kraft, D. D. C. Bradley, A. R. Brown, R. H. Friend, and R. W. Gymer, *Nature* **356**, 47 (1992).

20. M. Arnold, E. A. Cavalcanti-Adam, R. Glass, J. Blümmel, W. Eck, M. Kantlehner, H. Kessler, and J. P. Spatz, *ChemPhysChem* **5**, 383 (2004).

Chapter 5

Formation of self-assembled periodic grooves via thermal drawing lithography for alignment layers in liquid crystal devices

5.1 Introduction

Formation of periodic submicrostructures has many influential applications in science and technology, such as biomedical and opto-electric fields.[1,2] Thus, there are various kinds of nanolithography proposed to pattern polymer nanostructures. Electron-beam lithography and AFM nano-rubbing were often utilized to tailor the polymer surface, but the region of the pattern is very small and these techniques show very low throughputs.[3,4] Besides that, self-assembly by phase separation creating polymer periodic structure would produce multi-domains and hardly control the orientation of polymer pattern.[5] Some surface-modified lithography (like micro-contact printing) may contaminate the sample and limited to the selectivity between polymer

and self-assembly monolayer (SAM).[6,7] In this paper, we introduce and employ a low-cost and high throughput lithography - thermal drawing lithography (TDL) - to fabricate periodic self-assembled grooves. This remarkable lithography was discovered from the process of nanoimprint lithography.[8] TDL uses a prepatterned silicon mask (with periodic protrusions) which is mounted upon the bottom polymer face to face with a ~100 nm gap. Press the sandwiched structure and heat the whole set-up over the T_g of polymer. According to the image charge-induced electrohydrodynamic-instability (ICE) model, the attractive electrostatic force between the mask and polymer would cause heat-induced softened polymer film to rise and form grating patterns similar to the upper mask.[9] In our work, we have shown this extraordinary lithography could be achieved without an external electric field which is quite different from lithographically induced self-construction (LISC) and other researches.[10,11] In addition, the experimental results during TDL process support the ICE model. In the following experiments, we utilize self-assembled polymer grooves formed by TDL to align liquid crystal molecules. It is well-known LC molecules would tend to align parallel to the groove direction in order to make the LC elastic energy lowest.[12] Aligning LC molecules is a very important issue in manufacturing LC displays due to random-oriented LCs could not be a well light valve which controls light pass through or not properly. Though cloth rubbing polyimide is conventional method fabricating grooves for LC alignment, it still has some intrinsic problems, such as debris contamination, static electricity residual, high baking temperature (~250 ℃). AFM-assisted electrostatic nanolithography (AFMEN) has been investigated to establish polymer grooves.[13] However, the applying electric field is pretty large (~10^8 V m^{-1}) between the AFM tip and polymer film. Besides, the scanning rate of the tip should be slow to induce polymer formation. Here, TDL not only circumvents PI rubbing disadvantages but also realizes AFMEN in a large

area without scanning and applying an electric field. We successfully perform TDL on silicon and ITO substrates both to fabricate reflective and transmissive LC cells. The opto-electric properties of the LC cells are comparable, even prior, to other approaches which also aim to align LC molecules. Not only for LC displays, TDL fabricating nanostructures is also capable of many applications in other fields, such as polymer-based microelectronic circuits, microfluidic channels, and polymer resists for semiconductor lithography.[14-17]

5.2 Experiments and Discussions

5.2.1 Sample preparation

In material selectivity, amorphous polymer - which could change its glassy state to rubbery when the temperature is higher than T_g - is necessary for TDL experiments. Contrary to amorphous polymer, formation of polycrystalline polymer is more easily localized in a small domain and hard to stretch a large area with uniform pattern. Here, we choose polystyrene (PS, with a molecular weight of $M_w = 1.5$ kg mol^{-1}), a kind of amorphous polymer which is suitable for TDL. 1% (by weight) PS toluene solution was used to cast on silicon and ITO substrates to create a ~100 nm thickness film by the frequency of spin coating is 6000 rpm. Toluene solvent was driven off at 100 ℃. Then we utilized a silicon mold with a lateral 500 nm-width protruding grating as the upper
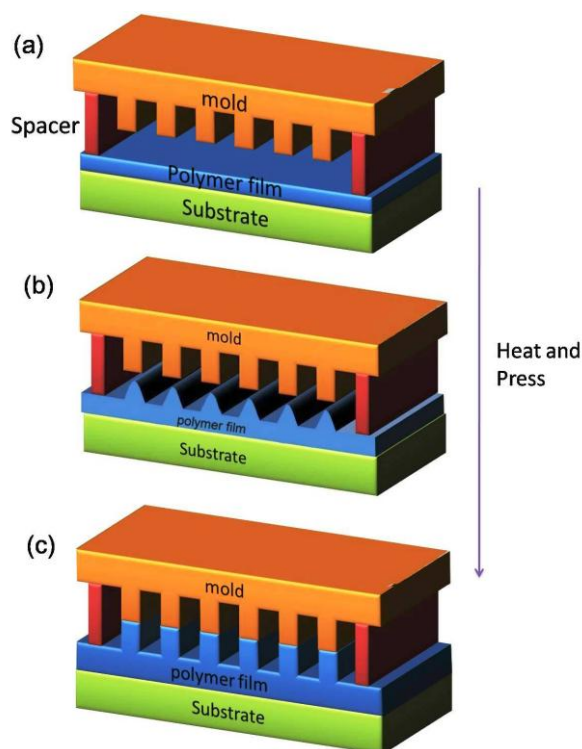
Figure 5.1 Schematic of self-assembled grooves formation using thermal drawing lithography.

mask. Before TDL, an aluminum spacer (~100 nm) was evaporated on the mask to provide a gap between polymer and the mask. Put the upper and bottom substrates together and apply a pressure to make the gap close to the spacer sustained (as shown in Figure 5.1(a)). In the mean time, heat the whole sandwich structure to elevate the temperature. In terms of the ICE model, the attractive electrostatic force between polymer and the upper mask would overcome the gravity and surface tension in thin liquid films to draw the softened polymer arising (Figure 5.1(b)). Pattern formations occur in polymer films at the temperature a little over the T_g of PS (115 ℃). As the heating time increased (~1 hour), the rising polymer grooves would contact with the

upper mask which makes the top of polymer grooves flat (Figure 5.1(c)). Before releasing the pressure and heat, the polymer grooves are immediately fixed by cooling the sample to room temperature. In this process, the clean surface and uniform gap is influential to carry out TDL. Figure 5.2 describes some special features that result from a nonuniform gap and no protrusion on the mask. The aesthetic phenomena as seen in Figure 5.2(a) looks like cloud pattern, local parallel stripes and partial concentric circles, observed in the polymer film which has too small space or even no gap between the upper and bottom substrates and is mechanically confined under a compressive stress, like NIL.[18] In Figure 5.2(b) and (c), the characteristic flowers and pillars patterns, which are called viscous fingers, are drawn from the featureless margin of the mask during TDL.[19] Some researches exhibit that the pillars pattern could be appropriately controlled into a hexagonal order.[9,21] Figure 5.3 shows an optical micrograph which polymer grooves with 500 nm-width extend to a large area via TDL (on the ITO substrate).

(a)   (b)   (c)
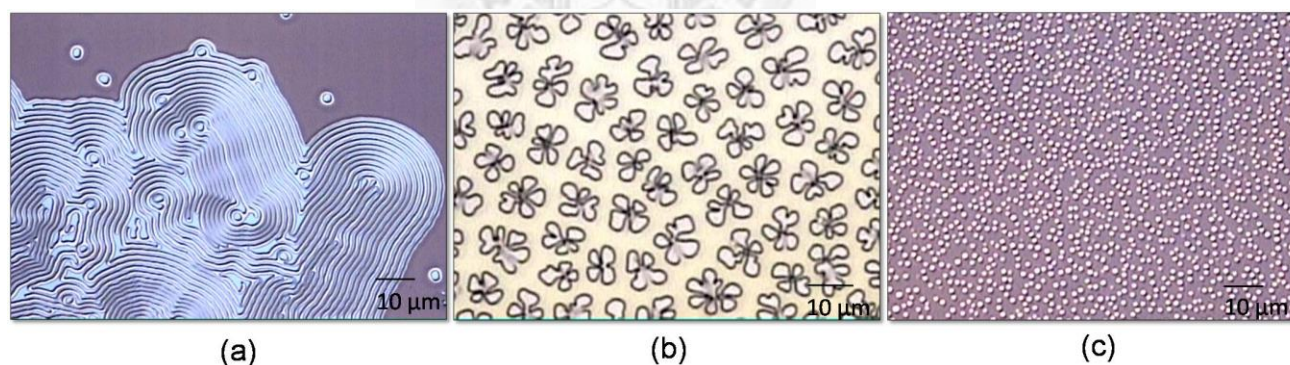
Figure 5.2   Some unexpected and special features resulted from TDL.

(a) The polymer film is mechanically confined under a compressive stress (with no spacer gap), like NIL.

(b) and (c) show the characteristic flowers and pillars patterns, which are called viscous fingers, are drawn from the featureless margin of the mask.
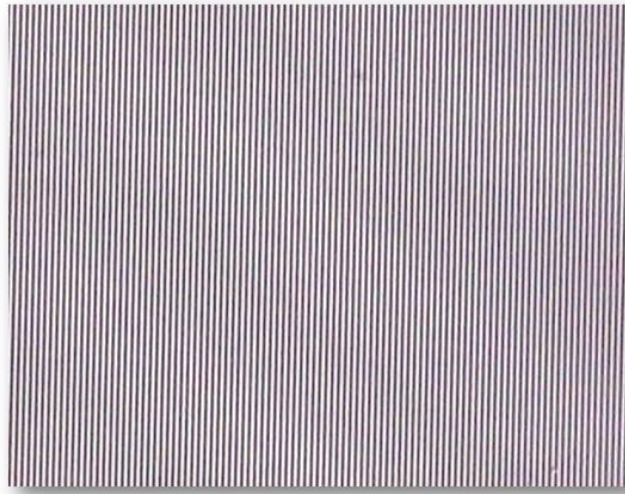
Figure 5.3 Optical micrograph of self-assembled PS grooves with line width ~500 nm uniformly stretching for a large area after the TDL method (on the ITO substrate).

(a)　　　　　　　　　(b)
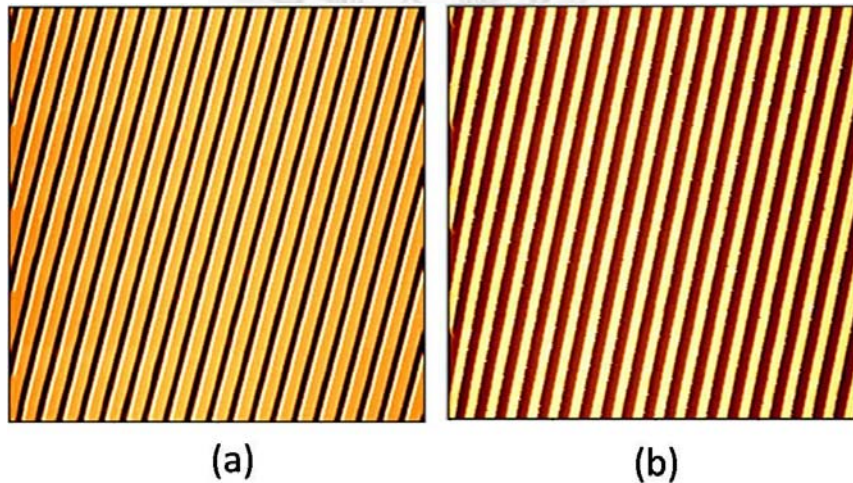
Figure 5.4 The morphology of TDL polymer grooves was investigated by AFM. (the widths of two images are both 20 μm)

(a) Polymer grooves with 500 nm width are formed on the ITO substrate.

(b) The TDL is also successful on the silicon substrate.

5.2.2 Observation and investigation of self-assembled polymer grooves

In our experiments, we perform TDL without any external electric field. This method is capable of applying on both ITO glass and silicon substrates. The morphology of TDL polymer grooves was investigated by AFM as shown in Figure 5.4. Fig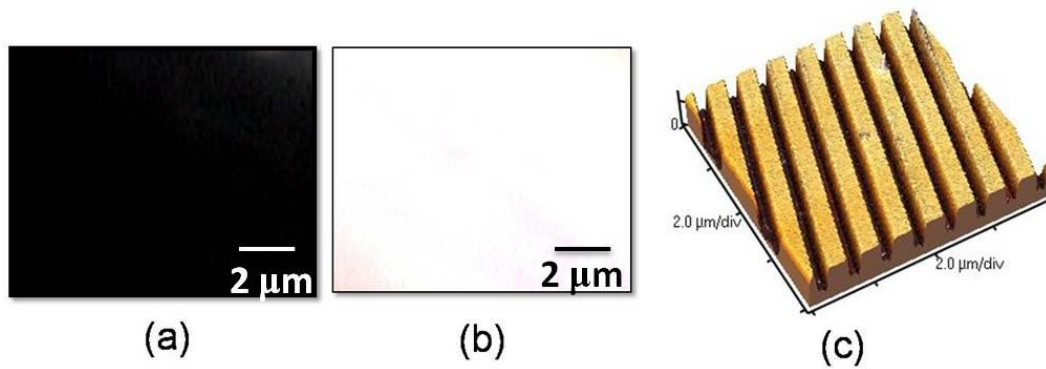ure 5.4(a) is polymer grooves on the ITO substrate, (b) is on the silicon substrate (the widths of two images are both 20 μm). Obeying the conservation of mass, the slight variation of film thickness which influences the polymer quantity is enough or not would affect the width of the rising part of grooves. The same influence would occur in different spacer gaps. On the other hand, the heating time determines the completion and perfection of the polymer grooves. Generally, the baking time is around 1 hour for a 100 nm spacer gap. As shown in Figure 5.5 (a), the cross-sectional image is the middle and instability situation of the process in which the baking time is less than 1 hour, then soon cooled and fixed its formation. Though the height of spacer is ~100 nm, the height of the induced grooves is only ~60 nm. The formation is illustrated in the inset. The charges accumulating at the corner on the upper grating attract the image charges in the melting polymer and cause two peaks on polymer grooves. These unexpected results coincide with the ICE model. Figure 5.5(b) is the sample heated by 1 hour with completely flat tops which result from the contact with the upper silicon mask. The height of grooves is ~100 nm which is consisted with the spacer's height. Higher gap would need much time to draw polymer grooves, but the result may turn all the previous efforts to nothing due to the spacer is too high. As the positive and negative charges are far away, the weaken electrostatics force is not large enough to compete with the gravity and polymer's surface tension.
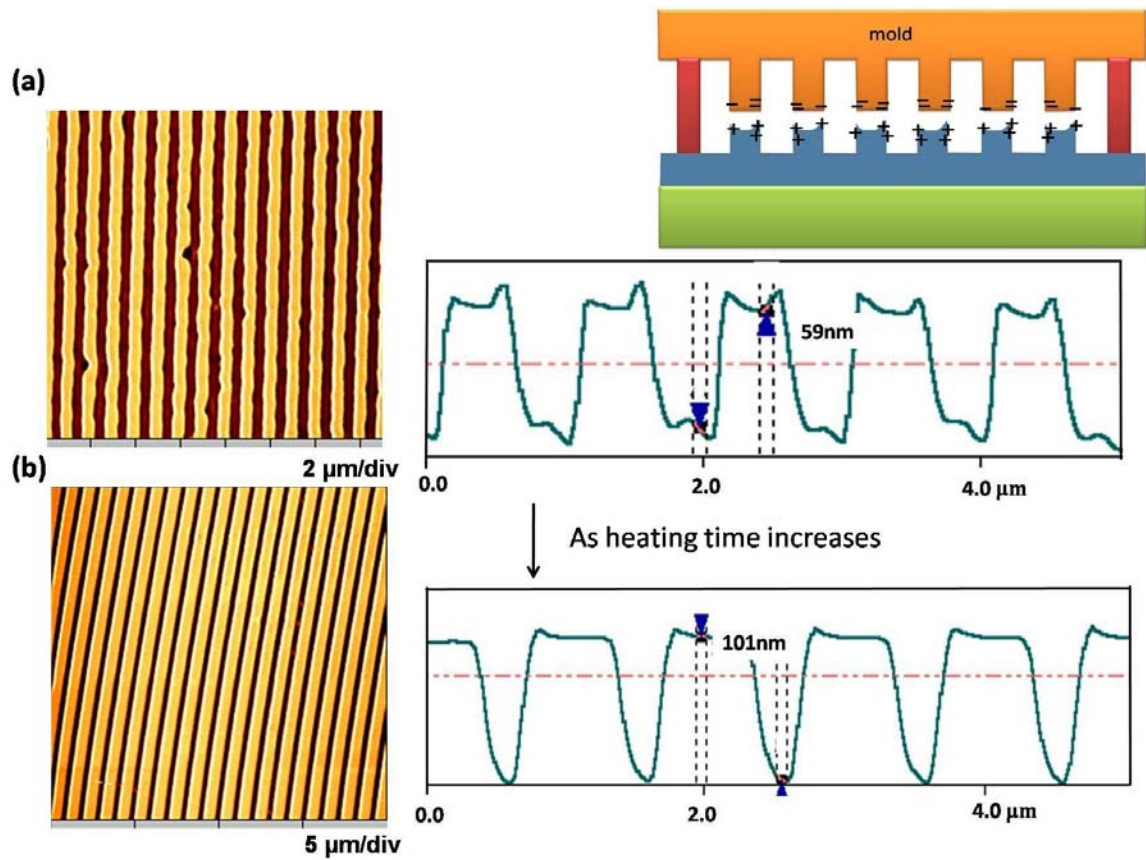
Figure 5.5

(a) The cross-sectional image shows the middle and instability situation of the process where the baking time is not enough. At this condition, the height of the induced grooves is lower than the height of the spacer (~100 nm). The inset is illustrated the ICE model.

(b) The sample is heated by sufficient time with completely flat tops which result from the contact with the upper silicon mask. The height of grooves is ~100 nm which is consistent with the spacer's height.
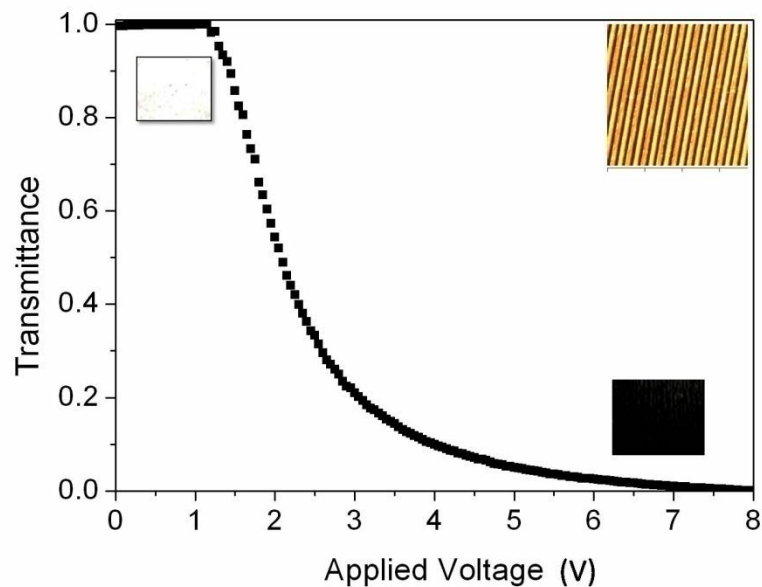
Figure 5.6

(a) The normally black mode of the MTN reflective LC cell (the line width ~500 nm, the height ~50 nm).

(b) With applied voltage, the LC cell became the bright state.

(c) The 3-dimensional morphology of polymer grooves on the silicon substrate.

5.2.3   Fabrication and measurements of liquid crystal cells

In the following, we utilized a silicon substrate and an ITO glass with TDL polymer grooves as the bottom substrates to fabricate the reflective and transmissive LC cells respectively. The bottom substrates were then covered by a conventional ITO glass coated with PI planar alignment layers as the upper substrates. The direction of TDL grooves was set orthogonal to the PI rubbing direction on the opposite substrate. Then, we filled this empty cell with a 5CB LCs at room temperature and the cell gap is 4 μm. Therefore, the director configuration of LCs sandwiched between the substrate with TDL grooves and the rubbed PI layer becomes twisted by 90° and we fabricated the MTN reflective cell and the TN transmissive cell.[21,22] The cells are inspected by a

polarizing optical microscope and the polarizer setting is demanded to obtain maximum darkness (or brightness) with zero voltage for the LC cell. Thus, the LC cell belongs to the normally black state (or normally white state). Figure 5.6(a) is the normally black mode of the MTN reflective LC cell (period ~1000 nm, height ~50 nm). Applying the voltage between the ITO layer and the p-type silicon substrate, the patterned LC cell, i.e. normally black mode, changed its phase retardation and became bright as seen in Figure 5.6(b). Figure 5.6(c) is the 3-dimensional morphology of polymer grooves on the silicon substrate. Figure 5.7 demonstrates the voltage-dependent light transmission (TV curve) of the transmissive TN-LC cell (The insets are the AFM image and optical micrographs). The threshold voltage which LCs started to change the phase retardation of this TV curve is around 1.3 V. As the applied voltage increased, the LCs orient along the electric field which results in the cell being the dark state between two crossed polarizers. Based on Berreman's theory, the anchoring energy resulted from grooves is $W = 2\pi^3 K A^2/\lambda^3$, which A is the amplitude, λ is the period of groove, and K is the Frank elastic constant of the LC ($K_{5CB} = 2 \times 10^{-12}$ N).[23] For the TN LC cell in Figure 5.7, with the period is ~800 nm and the amplitude is ~100 nm, the anchoring energy W is ~0.24×10^{-5} N m^{-1}. The anchoring energy of conventional PI rubbing is ~10^{-5} N m^{-1} and for AFM rubbing is ~10^{-6} N m^{-1}.[24,25] Thus, the anchoring energy of TDL polymer grooves between PI rubbing and AFM rubbing is enough to give a good control of LC molecules. The opto-electric properties perform well-comparable and could be more improved if the mask with a smaller-period grating is used.

Figure 5.7 The voltage-dependent light transmission (TV curve) of the transmissive TN-LC cell (The insets are the AFM image and optical micrographs). The threshold voltage of this TV curve is around 1.3 V. As the applied voltage increased, the LC cell became the dark state.

5.3 Summary

We have successfully carried out the thermal drawing lithography to form a periodic self-assembled polymer grooves. Besides, we have discovered some interesting results during the experimental process which could be explained by the ICE model. The TDL polymer grooves are utilized to align LC molecules and fabricated as an alignment layer of LC cells whose the opto-electric properties are well-performed and comparable, or prior, to other researches which also intend to align LCs. TDL is low

cost, low process temperature, and it does not have the residual static electricity and dust contamination. It avoids some disadvantages of conventional PI rubbing. In addition to grating pattern, TDL could create many intriguing micro- or nano-features and change its scale via a patterned mask or a totally flat mask. Importantly, not only for LC displays, TDL also provides a simple and feasible means to fabricate nanostructures which could be applied to many other fields, such as biosensors and opto-electric devices.

References

1 G. M. Whitesides, E. Ostuni, S. Takayama, X. Jiang, and D. E. Ingber, *Annu. Rev. Biomed. Eng.* **3**, 335 (2001).

2 P. L. Burn, A. B. Holmes, A. Kraft, D. D. C. Bradley, A. R. Brown, R. H. Friend, and R. W. Gymer., *Nature* **356**, 47 (1992).

3 D. M. Tennant, T. L. Koch, P. P. Mulgrew, R. P. Gnall, F. Ostermeyer, and J. -M. Verdiell, *J. Vac. Sci. Technol., B* **10**, 2530 (1992).

4 J. H. Kim, M. Yoneya, and H. Yokoyama, *Nature* **420**, 159 (2002).

5 D. E. Angelescu, J. H. Waller, D. H. Adamson, P. Deshpande, S. Y. Chou, R. A. Register, and P. M. Chaikin, *Adv. Mater.* **16**, 1736 (2004).

6 R. Jackman, J. Wilbur, and G. M. Whitesides, *Science* **269**, 664 (1995).

7 M. Böltau, S. Walheim, J. Mlynek, G. Krausch, and U. Steiner, *Nature* **391**, 877 (1998).

8 S. Y. Chou, P. R. Krauss, and P. J. Renstrom, *J. Vac. Sci. Technol. B* **14**, 4129 (1996).

9 S. Y. Chou and L. Zhuang, *J. Vac. Sci. Technol. B* **17**, 3197 (1999).

10 S. Y. Chou, L. Zhuang, and L. Guo, *Appl. Phys. Lett.* **75**, 1004 (1999).

11 E. Schäffer, T. Thurn-Albrecht, T. P. Russel, and U. Steiner, *Nature* **403**, 874 (2000).

12 F. C. Frank, *Discuss. Faraday Soc.* **25**, 19 (1958).

13 S. F. Lyuksyutov, R. A. Vaia, P. B. Paramonov, S. Juhl, L. Waterhouse, R. M. Ralich, G. Sigalov, and E. Sancaktar, *Nature Mater.* **2**, 468 (2003).

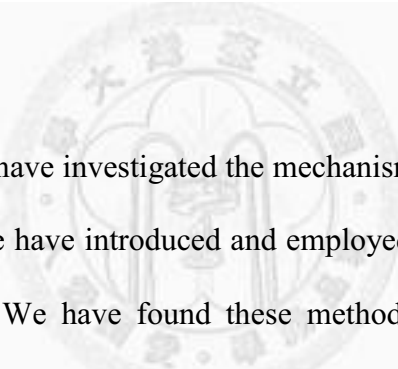14 Y. Xia, M. Mrksich, E. Kim, and G. M. Whitesides. *J. Am. Chem. Soc.* **117**, 9576 (1995).

15 R. Service, *Science* **278**, 383 (1997).

16 H. A. Stone, A. D. Stroock, and A. Ajdari, *Annu. Rev. Fluid Mech.* **36**, 381 (2004).

17 K. Mizoguchi and E. Hasegawa, *Polym. Adv. Technol.* **7**, 471 (1996).

18 J. Peng, Y. Han, Y. Yang, and B. Li, *Polymer* **44**, 2379 (2003).

19 A. Lindner, P. Coussot, and D. Bonn, *Phys. Rev. Lett.* **85**, 314 (2000).

20 P. A. Deshpande, PhD Dissertation Princeton University, 2005.

21 S. T. Wu, D. K. Yang, *Reflective Liquid Crystal Displays*, ed. A. C. Lowe, Wiley-SID, UK 2001, p. 89-108.

22 P. Yeh, C. Gu, *Optics of Liquid Crystal Displays*, ed. J. W. Goodman, John Wiley & Sons, Inc., US 1999, p. 123-124.

23 D. W. Berreman, *Phys. Rev. Lett.* **28**, 1683 (1972).

24 H. Yokoyama, *Mol. Cryst. Liq. Cryst.* **165**, 265 (1988).

25 J. H. Kim, M. Yoneya, J. Yamamoto, and H. Yokoyama, *Nanotechnology* **13**, 133 (2002).
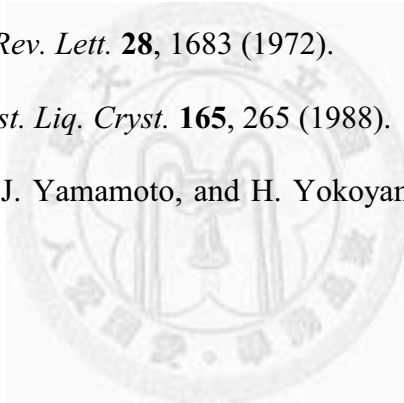
Chapter 6

Conclusion

In this dissertation, we have investigated the mechanism for aligning liquid crystals by surface relief grating. We have introduced and employed several nanolithography to fabricate periodic grooves. We have found these methods giving a good control of liquid crystals and they have given some insights into the basic physics of the alignment process. CAFM nanolithography not only provides a homogenous alignment precisely and generates an inorganic alignment layer avoiding the damage of UV exposure. It achieves a smaller pixel and a high resolution for LCDs. In the advanced research, thermal drawing lithography enlarges the pattern area of CAFM. It could induce polymer grooves without scanning an AFM tip which reduces the processing time and improves the throughput. During the thermal drawing lithography, we have discovered some interesting phenomena which could support the ICE model and explain the mechanism for the formation of thermal drawing lithography. Furthermore, we have disclosed the crack induced grooving method fabricating tunable-period grooves for LC

alignment. This novel and fascinating nanolithography is large-area, high-throughput, and low-cost. We are one of the leading groups performing this nanolithography successfully and putting it into practice.

More importantly, these alignment methods not only prevent scratching damage, dust contamination and residual static electricity caused by conventional cloth rubbing, but also avoids the high baking temperature in manufacturing LCDs. Compare to the other approaches, these methods have comparable, even better, electro-optical properties and anchoring energy. More than successfully aligning LCs, these methods generating surface relief grating could align or sort other molecules for applications of biochips, microchannels, polarizers, etc. They also provide an alternative comparable to the existing mainstream LCD technologies and hold promising potentials for many opto-electric devices.